Task 11. University of California, Berkeley (Subcontract)

The objective of this task is the characterization of the structure and function of active sites involved in the synthesis of high molecular weight hydrocarbons from CO and H_2 on multi-component catalysts based on Fe as the active component.

Table Of Contents

I. FISCHER-TROPSCH SYNTHESIS ON IRON CATALYSTS

1. Background

1.1. Structure and Function of Active Phases in Fischer-Tropsch Synthesis

Fe-based oxides have been used as commercial catalysts for Fischer-Tropsch synthesis (FTS) to produce a wide range of paraffin and olefin products, ranging from methane to high molecular weight waxes [1]. During activation in synthesis gas and subsequent FTS reaction, several phases including metallic iron, iron carbides and iron oxides can co-exist at steady-state conditions [2-5]. The relative amounts of these phases depend on various activation and reaction conditions, which also lead to different catalytic performance. Some researchers [6] have proposed that surface iron atoms are responsible for FTS activity, while others have considered surface carbides or a mixture of carbides [7,8] with metallic iron [9] to be the active phase. There are also some reports that suggest that magnetite Fe_3O_4 is the active FTS phase [10-12]. Although these studies have each provided some evidence to support its specific proposal about the active phase, the available information remains phenomenological and sometimes contradictory, and a direct method to identify the active phase during reaction and to count the number of active sites has remained elusive. Based on our previous studies of the active phases and catalytic activity of Fe-Zn-K-Cu oxides [18-25], we have summarized in this reporting period with three manuscripts that address the structure and site requirement for Fe-based FTS catalysts.

1.2. Effects of Zn, Ru (Cu) and K on Fe Oxides

Many components have been incorporated into Fe catalysts in order to improve their mechanical and catalytic properties. Our previous studies have shown that Zn, K and Cu [13-15] promote the catalytic properties of Fe oxides. Zinc oxide, as a non-reducible oxide at FTS conditions, appears to stabilize the surface area of Fe oxide precursors. Alkali, as a modifier of the adsorption enthalpies of H_2 and CO, has been reported to increase the selectivity to desired C_{5+} products. Copper promotes the carburization processes and decreases the temperature required for the activation of iron oxide precursors. According to our previous optimum composition of Fe-Zn-K-Cu (Zn/Fe=0.1, K/Fe=0.02, Cu/Fe=0.01), we have prepared a series of Zn and Fe co-precipitated oxides with constant Zn/Fe and K/Fe atomic ratios (Zn/Fe=0.1, K/Fe=0.02) and varying amounts of Ru (Ru/Fe=0-0.01). Ru is a very active FTS catalyst. Ru was chosen in order to improve the catalytic activity and to minimize unfavorable water gas shift reactions, which can be catalyzed by the Cu component on Fe catalysts. Also, K was added in order to increase wax and alkene yields, while decreasing the production of undesirable methane products. The same effects of K are expected on Fe-Zn-Ru-K catalysts. The effect of K and Cu on the reduction/carburization and FTS reactions has been discussed in detail in the manuscripts.

2. Synthesis Procedures

2.1 Higher Surface Area Fe-Zn-K-Cu Oxides

Fe-Zn-K-Cu catalysts were prepared by co-precipitation of iron and zinc nitrates following the procedure described in our previous report [18]. In order to produce high surface area samples, an alcohol (isopropanol or ethanol) was used instead of water in order to wash the precipitates before drying. Isopropanol or ethanol was employed to reduce the pore mouth pinching caused by the surface tension of intrapore liquids during drying. Since the subsequent impregnation of an aqueous solution of $K_2(CO_3)$ and $Cu(NO_3)_2$ introduces a substantial amount of water back into the precursors, which becomes the major cause for decrease of surface areas during second dryings, we dissolved $K_2(CO_3)$ and $Cu(NO_3)_2$ using the least amount of water and diluted the solution using isopropanol or ethanol to obtain a liquid volume required for incipient wetness impregnation. Then, the dried materials were treated in dry air at 543 K for 4 h. A larger amount of K (K/Fe=0.02-0.08) and Cu (Cu/Fe=0.02-0.04) were doped to the Fe-Zn oxide precursors in order to match their higher surface areas obtained by alcohol-wash and to maintain a constant surface density (atoms/nm^2) on these materials.

2.2. Fe-Zn-Ru-K Oxides

The preparation of the Fe-Zn-K-Ru catalysts used in this reporting period have been described in the previous quarterly report (25).

3. Catalyst Characterization

3.1. Protocols for the Characterization of Fe-based FTS Catalysts

This research program addresses the synthesis and the structural and catalytic characterization of active sites in Fe-based catalysts for FTS. We have designed a matrix of samples consisting of a systematic range of multicomponent catalysts in order to determine the number and type of surface sites present on fresh catalysts and on samples during and after FTS reaction (Table 1.1). Our objective is to develop rigorous relationships between the synthesis methods, the resulting catalyst structures, and their function in FTS reactions.

4. Structure and Site Requirement of Fe-Zn-K-Cu Oxides for Fischer-Tropsch Synthesis

The reduction, carburization, and catalytic properties of Fe-Zn-K-Cu(Ru) oxides catalysts were examined using kinetic and spectroscopic methods at FTS conditions. The structure and site requirements for FTS reactions and the effect of K and Cu were discussed in the following manuscript.

Table 1.1. Matrix of samples and characterization methods for FTS reaction

<table>
<tr><th colspan="3">Nominal Composition of the Catalysts</th><th rowspan="2">Characterization Before and After FTS</th><th rowspan="2">FTS reaction</th></tr>
<tr><th>Zn/Fe mole ratio</th><th>K/Fe (at.%)</th><th>Cu/Fe (at.%)</th></tr>
<tr><td rowspan="6">0</td><td rowspan="2">0</td><td>0</td><td rowspan="24">XRD

Surface area

In situ XAS

H_2-TPR

CO-TPR

Isotopic transient</td><td rowspan="24">Effect of reaction condition

493 K
2140 kPa

508 K
2140 kPa

543 K
500 kPa

Effect of CO_2 addition

Isotopic studies</td></tr>
<tr><td>1</td></tr>
<tr><td rowspan="3">2</td><td>0</td></tr>
<tr><td>1</td></tr>
<tr><td>2</td></tr>
<tr><td>4</td><td>1</td></tr>
<tr><td rowspan="2">0.05</td><td>0</td><td>0</td></tr>
<tr><td>2</td><td>1</td></tr>
<tr><td rowspan="8">0.1*</td><td rowspan="2">0</td><td>0</td></tr>
<tr><td>1</td></tr>
<tr><td rowspan="3">2</td><td>0</td></tr>
<tr><td>1</td></tr>
<tr><td>2</td></tr>
<tr><td rowspan="2">4*</td><td>1*</td></tr>
<tr><td>2*</td></tr>
<tr><td>6*</td><td>3*</td></tr>
<tr><td rowspan="2">8*</td><td>2*</td></tr>
<tr><td>4*</td></tr>
<tr><td rowspan="2">0.2</td><td>0</td><td>0</td></tr>
<tr><td>2</td><td>1</td></tr>
<tr><td rowspan="3">0.4</td><td>0</td><td>0</td></tr>
<tr><td>2</td><td>1</td></tr>
<tr><td>6</td><td>2</td></tr>
<tr><td>Zn/Fe</td><td>Ru/Fe (at.%)</td><td>K/Fe (at.%)</td></tr>
<tr><td rowspan="4">0.1</td><td>0.5</td><td rowspan="2">0</td></tr>
<tr><td>1</td></tr>
<tr><td>0.5</td><td rowspan="2">2</td></tr>
<tr><td>1</td></tr>
<tr><td rowspan="4">0.1*</td><td>0.5*</td><td rowspan="2">0*</td></tr>
<tr><td>1*</td></tr>
<tr><td>0.5*</td><td rowspan="2">2*</td></tr>
<tr><td>1*</td></tr>
</table>

* Samples treated by alcohol-wash.

4. Catalyst Design and Control of Site Density for Fe-Based Fischer-Tropsch Synthesis

Abstract

A step-by-step approach to the design of high activity Fe-based Fisher–Tropsch synthesis (FTS) catalysts was applied by using promoters such as K, Cu and Ru to control the site density of active Fe carbide species. The effect of these promoters on the reduction/carburization, the catalytic activity, and the site density of Fe-Zn oxides, was examined using a combination of kinetic and spectroscopic probe methods. The presence of promoters increased the reduction/carburization rates of Fe-Zn oxide precursors and also increased the FTS rates, which corresponded to an increase in the density of active sites measured after activation and FTS reactions using a CO site titration technique. The consistent correlation between the FTS rates and the density of CO binding sites on promoted Fe catalysts indicates that the effect of each promoter is to produce a larger number of nucleation sites for the formation of smaller FeC_x crystallites. These in turn led to higher density of active sites for CO adsorption/dissociation, promoted carburization, and hence increased FTS rates. These results offer a consistent and tenable interpretation about the effect of promoters on the FTS performance of Fe catalysts, which has been explained by many confusing and sometimes contradicting chemical effects. In an effort to enhance the site density by increasing the surface area of the Fe oxide precursors, a high surface area Fe-Zn-K-Cu oxide catalyst was prepared using an alcohol instead of water as the surface-active component, to wash the Fe-Zn hydroxide precursors in order to minimize their decrease in surface areas due to the pore mouth pinching caused by the surface tension of intrapore liquids during the drying process. The resulting highly dispersed Fe-Zn-K-Cu catalyst, when compared with a typical Co/SiO_2 catalyst at conditions normally employed for Co-FTS catalysts, showed similar hydrocarbon productivities. This observation clarifies the misunderstanding that Co is more active than Fe catalysts for FTS reactions. In fact, Fe-based catalysts, which are significantly less sensitive to FTS reaction conditions than Co catalysts, if prepared highly dispersedly with appropriate choice of synthesis protocols, can provide active and selective alternative to Co catalysts.

Introduction

Fe-based catalysts provide an attractive complement to Co-based catalysts for the Fischer-Tropsch synthesis (FTS) reactions. They lead to the production of more olefinic hydrocarbons and lower CH_4 selectivities than Co catalysts over a wide range of temperatures and H_2/CO ratios, including synthesis gas derived from coal and biomass feedstocks (1). Cobalt catalysts are generally considered to be more active; they must be used, however, at low temperatures (470-490 K), because the selectivity to the desired C_{5+} products and the quality of the diesel range products becomes unsatisfactory at higher temperatures (2). The apparent lower FTS rates on Fe-based reflect to some extent the lower dispersion of the active component in these FTS catalysts. Thus, increasing their dispersion and surface area during synthesis and during the initial stages of use in activating or reaction mixtures provides an attractive approach to bring Fe-based catalysts into the activity and operating regimes of Co-based catalysts (3). The resulting opportunities to use Fe-based catalysts at low temperatures would favor even heavier hydrocarbons and a lower selectivity to CO_2. Also, it would allow direct comparisons of FTS turnover rates on Fe and Co catalysts at identical low-temperature conditions. Such comparisons would require, however,

measurements of the number of exposed active components in both catalysts. These measurements are widely used for Co catalysts, but not for Fe-based catalysts, which activate to form complex mixtures of oxide and carbide phases during Fischer-Tropsch synthesis.

Here, we report the design and synthesis of Fe-based catalysts with hydrocarbon synthesis productivities similar to those on Co-based materials. We also report direct comparisons of turnover rates on these two types of catalysts, made possible by a method developed to count the number of CO binding sites on Fe catalysts after activation and reaction. Our previous studies of the catalytic properties of Fe (4) or Fe-Zn (5) catalysts have shown that FTS rates increased with K or Cu addition, and the rate was highest when both K and Cu were added (6). These promotional effects reflect largely the formation of Fe carbides with higher dispersion when K or Cu is present. Our initial attempt to improve the density of active sites in these materials and to decrease the CO_2 selectivity led us to replace Cu, the active component in the best available water-gas shift (WGS) catalysts (7), with Ru. Ru was chosen because it does not introduce undesired methanation side reactions and has been explored as an active, but impractical, FTS catalyst (8), and as a promoter for Co-based catalysts (9). Ru increased FTS rates more effectively than Cu at similar atomic contents and without detectable changes in chain growth selectivity. As in the case of Cu, Ru predominately increased the density of active sites by favoring the nucleation of smaller Fe carbide and Fe_3O_4 domains during the conversion of Fe_2O_3 precursors to active catalysts in the initial stages of FTS reactions. This conclusion was confirmed by surface area, CO chemisorption, and isothermal transient experiments. These smaller crystallites, in turn, provided higher surface areas, shorter bulk diffusion distances, more complete carburization of Fe_2O_3 precursors, and higher steady-state FTS rates. Higher FTS rates were also achieved by synthetic protocols leading higher precursor surface areas. These led to a higher dispersion of Fe_2O_3 precursors, which was maintained during its activation, especially when decomposition and activation procedures were designed in order to minimize the sintering of these high surface area oxide precursors.

Finally, the catalytic activity of the FTS reactions at the operation conditions for Co catalysts (H_2/CO=2, 473 K) on a high surface area Fe-Zn-K-Cu oxide catalyst was compared with that of a Co/SiO_2 catalyst studied previously (10). Our results show that turnover rates are higher on exposed Co surface atoms than on Fe-based active sites. Fe-based catalysts designed with a high density of CO binding sites, however, can lead to similar and even higher hydrocarbon synthesis productivities and to lower CH_4 selectivities than Co-based FTS catalysts.

Experimental

Catalyst Preparation

Fe-Zn oxide precursors were prepared by co-precipitation from a mixed solution of Fe and Zn nitrates using ammonium carbonate as the precipitating solution. A solution mixture containing $Fe(NO_3)_3$ (Aldrich, 99.9+%, 3.0 M) and $Zn(NO_3)_2$ (Aldrich, 99.9+%, 1.4 M) at a Zn/Fe atomic ratio of 0.1, was added at a rate of 120 cm^3/h using a liquid pump into a large flask containing deionized water (~100 cm^3) at 353 K. $(NH_4)_2CO_3$ (Aldrich, 99.9%, 1 M) was added separately to this flask at the rate required to maintain the pH of the resulting slurry at a constant value of 7.0±0.1, as measured by a pH meter (Omega, PHB-62). The precipitates (~20 g) were washed five times with doubly distilled deionized water (~ 200 cm^3/g each time), dried in ambient air at

393 K overnight, and then treated in flowing dry air at 623 K for 1 h. The K, Cu, and Ru promoters were added to these Fe-Zn oxide precursors by impregnating them to incipient wetness with aqueous solutions of K_2CO_3 (Aldrich, 99.99%, 0.16 M), $Cu(NO_3)_2$ (Aldrich, 99.99%, 0.16 M), or ruthenium (III) nitrosyl nitrate [$Ru(NO)(NO_3)_x(OH)_y$ (x+y=3)] (Aldrich, solution in dilute nitric acid, Ru 1.5%) at the concentrations required to obtain the desired K/Fe and Cu or Ru/Fe atomic ratios (K/Fe=0.02, Cu/Fe=0.01). The impregnated samples were then dried 373 K in ambient air. Finally, the samples were treated in a flow of dry air at 673 K for 4 h. The resulting oxide precursors are denoted throughout as Fe-Zn-K_2, Fe-Zn-K_2-Cu_1 and Fe-Zn-K_2-Ru_1, respectively. The subscripts denote the atomic percentages of the corresponding promoters.

High surface area Fe-Zn-K-Cu oxide precursors were prepared using surface-active components, such as alcohols, in order to minimize the pore mouth pinching caused during drying by high surface tension intrapore liquids. Fe-Zn-K_4-Cu_2 oxides were prepared by the procedure described above, except that alcohols (isopropanol or ethanol) were used instead of water to wash the porous solids after precipitation and before drying. In order to maintain similar promoter surface densities on these higher surface area oxides, proportionately higher concentrations of K (K/Fe=0.04) and Cu (Cu/Fe=0.02) were introduced by incipient wetness impregnation. After co-precipitation, the powders were washed with isopropanol or absolute ethanol (Fischer Chemical) five times (~200 cm^3/g each time) at room temperature. Magnetic stirring was used during the washing procedure in order to increase the rate at which intrapore liquid water was replaced by the alcohol.

A Co/SiO_2 catalyst containing 21.9 wt.% Co was prepared by incipient wetness impregnation of SiO_2 (Grace-Davison; grade 62) with a solution of cobalt nitrate (Aldrich, 98%, 2.5 M) followed by drying at 333 K and a H_2 pretreatment procedure that has been described previously (11). This sample showed a Co dispersion of 4.6% using H_2 chemisorption methods and its FTS turnover rates at standard conditions (473 K, 2 MPa) was 46-73 h^{-1}. This performance places it within the range of turnover rates for the best Co-based catalysts reported in the literature (10).

Fischer-Tropsch Synthesis Rates and Selectivities

FTS reaction rates and selectivities were measured on both Fe and Co catalysts using a fixed-bed, single-pass flow reactor with plug-flow hydrodynamics. This reactor was contained within a three-zone furnace controlled by three temperature controllers (Watlow, Series 982 and 988). Tubular reactors were constructed of stainless steel (SS 304, 1.27 cm outer diameter and 1 cm inner diameter for Fe catalysts; 0.95 cm outer diameter and 0.5 cm inner diameter for Co catalysts). Axial temperature profiles were measured using a type K movable thermocouple. The temperatures at all bed positions were within ±0.5 K of the average temperature. All lines after the reactor were kept at 433-553 K and a vessel placed immediately after the reactor was held at 408 K. Another vessel was placed at ambient pressure and temperature after a sampling valve that collected gaseous components (at ambient pressure and 523 K) for injection into a gas chromatograph.

Fe catalysts (100~180 μ, 0.4 g) were diluted with 11 g of quartz granules in order to avoid temperature gradients. These quartz granules were washed with concentrated nitric acid and calcined at 973 K prior to use. This catalyst was activated using flowing synthesis gas

(H_2/CO=2) at 0.1 MPa by increasing the temperature from 298 K to 423 K at a rate of 0.167 K/s and from 423 K to 543 K at 0.017 K/s. The catalyst was held at 543 K for 1 h and the synthesis gas pressure was increased to 2 MPa. The Co catalyst (100~180 μ, 1.06 g) was diluted with the SiO_2 support (3 g) used to prepare this sample. It was reduced in pure H_2 (Airgas: 99.99% H_2, 0.538 mol/g-s) by increasing the temperature from 298 K to 598 K at 0.167 K/s and holding at 598 K for 1 h. After reduction, the temperature was decreased to 473 K, synthesis gas was introduced, and the pressure was increased to 2 MPa gradually.

Synthesis gas was a H_2/CO/N_2 mixture (0.62/0.31/0.07 mole fractions; Praxair: 99.9% H_2, 99.9% CO, 99.99% N_2). N_2 was used as an internal standard in order to ensure accurate mass balances. This reactant mixture was purified using activated carbon (Sorb-Tech RL-13) to remove metal carbonyls, and molecular sieve (Matheson, Model 452A) to remove water. All flows were metered using mass flow controllers (Porter, Model 201-AFASVCAA or Brooks, Model 5850-CAB1AF1A3). Reactant and product streams were analyzed on-line using a gas chromatograph (Hewlett Packard, Model 5890 Series II) equipped with a 10-port sampling valve and two sample loops. The contents of one sample loop were injected into a cross-linked methyl silicone capillary column (HP-1, 50 m × 0.32 mm; 1.05 μ film); and the contents of the other loop were injected into a Porapak Q (15.2 cm × 0.318 cm) packed column. Ar, N_2, CO, CO_2, and light hydrocarbons eluting from the packed column were analyzed using a thermal conductivity detector (TCD). A flame ionization detector (FID) was used to analyze all hydrocarbon products as they eluted from the capillary column. The concentrations of all hydrocarbons up to C_{15} were measured using these chromatographic protocols.

Temperature-Programmed Reduction/Carburization of Fe-Zn-K-Cu(Ru) Oxides in H_2 or CO

The reduction and carburization kinetics of promoted Fe-Zn oxide precursors were examined by temperature-programmed reaction (TPR) using H_2 and CO as reactants. Samples (0.2 g, 100~180 μ) were placed within a quartz cell (10 mm i.d.), supported on a quartz frit as a thin packed bed, heated in 20% O_2 in Ar (0.268 mol/h) to 673 K at 0.33 K/s, and held at 673 K for 0.2 h in order to remove H_2O before reduction or carburization experiments. The samples were then cooled to ambient temperature in Ar and the gas stream switched to 20% H_2/Ar or 20% CO/Ar (0.268 mol/h). The reactor temperature was then increased to 1000 K at 0.167 Ks^{-1}. A part of the effluent stream (~40 %) was introduced into a differentially pumped atmospheric sampling system connected to a quadrupole mass spectrometer (Leybold Inficon Instruments Co., Inc.) to measure the concentration of CO or H_2 reactants and of any reduction and carburization products.

In Situ X-ray Absorption Measurements

Fe K-edge X-ray absorption spectra were measured at the Stanford Synchrotron Radiation Laboratory (SSRL) using a wiggler side-station (beamline 4-1). During these experiments, the storage ring was operated at 30-100 mA and 3.0 GeV. Two Si (111) crystals detuned by 20% in order to minimize harmonics were used as the monochromator. The intensities of the X-ray beam incident on the sample (I_0), after the sample (I_1), and after a 5 μ Fe calibration foil (I_2), were measured by three N_2-filled ion chambers and the sample (I_0/I_1) and reference (I_1/I_2) spectra were simultaneously obtained. The most restrictive aperture along the beam path was the 0.2×12 mm

slit within the hutch, which provided better than 2 eV resolution at the Fe K-edge (7.112 keV) (12). The catalyst samples (100~180 μ) diluted to 10 wt.% Fe using graphite powder (Alfa AESAR, 99.9995%, S_g< 1 m^2/g, 180-250 μ) were placed within an *in situ* quartz capillary cell (4). Analysis of X-ray absorption data was performed using WinXAS (version 1.2) (13). Calibration of raw spectra was achieved by the alignment of the first inflection point in the Fe foil spectrum with the known absorption energy of Fe^0 (7.112 keV). Background subtraction was performed using linear fits for the pre-edge region (6.900-7.100 keV) and a sixth-order polynomial fit for the post-edge region (7.240-8.120 keV). Principal component analysis (14) and linear combination methods (15) were used to calculate the relative abundance of the various Fe phases, using the near-edge spectral region between 7.090 and 7.240 keV for each sample and for Fe reference compounds. The details of the approach used to identify and quantify Fe species formed during FTS reactions have been described elsewhere (4).

Fischer-Tropsch Synthesis Reaction Rate Measurements

Isothermal transient experiments were used to measure product formation rates during FTS at conditions identical to those used for the *in situ* X-ray absorption studies. 0.2 g of the sample (100~180 μ) was diluted with graphite (0.5 g, 180-250 μ, Alfa AESAR, 99.998%) and placed in a quartz microreactor. It was then treated in He (Matheson, 99.999%, 0.268 mol/h) at 573 K for 0.2 h and cooled in He to 523 K. The He stream was then replaced with synthesis gas at 523 K (H_2/CO/Ar: 0.40/0.20/0.40 mole fractions; 0.1 MPa; Matheson, 99.999%, 0.268 mol/h). The resulting isothermal transients in the rate of evolution of several FTS products (e.g., CH_4, H_2O, CO_2, etc.) were measured as a function of time using on-line mass spectrometry. The rate of CH_4 formation was used as a surrogate measure of total FTS rates, because it can be measured accurately, and it changes with time on-stream in parallel with the rate of formation of higher hydrocarbons. CH_4 selectivities change with time on stream by less than 5%; therefore, CH_4 formation rates accurately reflect the total rate of hydrocarbon synthesis.

CO Chemisorption and Surface Area Measurements

Catalyst samples (0.2 g, 100~180 μ, diluted with graphite) were treated in flowing He (0.268 mol/h) up to 573 K and then cooled down to 523 K. The flow was switched to synthesis gas (H_2/CO/Ar: 0.40/0.20/0.40 mole fractions; 0.1 MPa; Matheson, 99.999%, 0.268 mol/h) at 523 K for 1 h. Reversibly adsorbed species were removed by flowing He (0.268 mol/h) at 523 K for 1 h. Following these steps, the samples were cooled to ambient temperature, and CO chemisorption and BET surface area measurements were then performed.

Two types of CO temperature-programmed desorption (TPD) experiments were carried out. A flow of CO/Ar stream (0.02/0.08 MPa; 0.268 mol/h) was passed through the sample for 0.5 h in one type of experiment. This was followed by the removal of weakly adsorbed species by flowing Ar (Matheson, 99.999%, 0.268 mol/h) at RT for 0.5 h. The samples were then heated to 1000 K at 0.167 K/s and the evolution of CO_x species ($CO+CO_2$) in Ar flow (0.268 mol/h) was measured by mass spectrometry. The other type of measurement involved a similar procedure but without a CO chemisorption step after FTS. The difference between the peak areas under these two TPD curves was taken as a measure of the availability of active sites capable of chemisorbing CO reversibly at FTS temperatures. This allowed the subtraction of those CO

species formed from irreversibly adsorbed carbon species present during FTS from the total CO evolved, as well as any CO_x formed by reactions of carbidic carbon with residual Fe oxides at temperatures much higher than those prevalent during FTS reactions.

BET surface area measurements were carried out after FTS reactions at 523 K, quenching to ambient temperature, and passivating catalyst samples in flowing 1% O_2/He at RT. N_2 physisorption measurements were performed at its normal boiling point (77 K) using an Autosorb 6 system (Quantachrome, Inc.). Surface areas were calculated using the BET method.

Results and Discussion

Comparison of the Reduction and Carburization Behaviors of Ru- and Cu-promoted Fe-Zn-K oxides

Figure 1 shows oxygen removal rates for the Fe-Zn-K-Cu(Ru) oxide samples as a function of temperature during exposure to H_2. The amount of oxygen removed in each of the two major reduction peaks indicates that the reduction of Fe-Zn-K-Cu(Ru) oxides follows similar sequential reduction steps observed for Fe_2O_3 (5), which reduces to Fe_3O_4 and then to Fe in two distinct kinetic steps. The addition of Cu to Fe-Zn-K oxides led to incipient reduction at temperatures ~130 K lower than on the Cu-free sample (Figures 1a and 1b), as a result of H_2 dissociation sites provided by the reduction of CuO to Cu metal at low temperatures. Ru had similar but stronger effects on the temperature required for reduction of Fe_2O_3 to Fe_3O_4 and of Fe_3O_4 to Fe (by an additional 50 K and 100 K, respectively). It appears that Ru, because of its higher metal dispersion, or lower reduction temperatures, or higher H_2 dissociation turnover rates, leads to greater availability of hydrogen at lower temperatures than for oxide precursors with similar atomic Cu content.

Figure 2 shows oxygen removal and carbon introduction rates for Fe-Zn-K-Cu(Ru) oxides as a function of temperature using CO as the reducing and carburizing agent. Fe-Zn-K-Cu(Ru) oxides convert *via* reduction/carburization steps similar to those observed for pure Fe_2O_3 (5). Fe_2O_3 reacts with CO to form Fe_3O_4 and the latter then reduces and carburizes simultaneously to form a mixture of $Fe_{2.5}C$ and Fe_3C, denoted here as FeC_x and confirmed by X-ray diffraction (5). The temperature required for these reduction-carburization processes is lowest for Fe-Zn-K_2-Ru_1 and highest for the sample without either Cu or Ru (Fe-Zn-K_2). Ru-promoted samples reduced and carburized at temperatures ~30 K lower than Cu-containing samples. The promoting effects of Ru and Cu on reduction and carburization by CO were weaker than their respective effects on the reduction of Fe oxide precursors using H_2, but Cu and especially Ru clearly promoted the removal of oxygen using CO as the reductant. The effect of Ru and Cu on the rate of reduction and carburization of Fe-Zn oxide precursors suggests that these components increase the initial rate of nucleation of reduced Fe-containing phases (Fe_3O_4, FeC_x). The resulting larger number of nuclei is likely to lead to a better dispersion of these reduced phases, as shown in earlier studies (4), and to a larger number of active sites for Fischer-Tropsch synthesis reactions. This expectation was confirmed by the catalytic performance measurements of these materials, as reported in the next section.

Effect of Ru and Cu on Fischer-Tropsch Synthesis Rate and Selectivity

Fischer-Tropsch synthesis rates were measured on Fe-Zn-K_2, Fe-Zn-K_2-Cu_1, and Fe-Zn-K_2-Ru_1 samples at 508 K and 2.14 MPa. Measurements were conducted at different CO space velocities and steady-state hydrocarbon formation rates (mol CO/h.g-at.Fe) are shown as a function of the resulting extent of CO conversion in Figure 3a. These rates were higher on the Ru-promoted sample (Fe-Zn-K_2-Ru_1) than on Cu-promoted (Fe-Zn-K_2-Cu_1) or unpromoted (Fe-Zn-K_2) catalysts, but the effects of increasing conversion on FTS rates were similar on all samples, suggesting similar kinetic dependencies on reactant and product concentrations. Ru and Cu appear to increase the number of active sites available on catalysts derived from Fe-Zn oxide precursors, without any detectable changes in the turnover rates or kinetics of chain growth or CO hydrogenation on the active sites or in the pathways available for these reactions. This is consistent with the nearly identical selectivities to C_{5+} (Figure 3c) and CH_4 (compared in Table 1 at nearly equal CO conversions), and the similar α-olefin/*n*-paraffin ratios (Figure 3d) on all catalysts at all conversion levels.

CO_2 selectivities increased with CO conversion on all three catalysts (Figure 3b). They were higher on Cu- or Ru-promoted Fe-Zn-K oxides than on unpromoted catalysts at all conversion levels. The slope of the CO_2 selectivity-CO conversion curves in Figure 3b are similar on all three catalysts, suggesting that the rate of secondary water-gas shift reactions are not influenced by the promoters, even though high water-gas shift rates have been reported on Cu-based catalysts (7). The extrapolated y-intercepts in Figure 3b reflect the relative rates of removal of chemisorbed oxygen, formed in CO dissociation steps, using CO or hydrogen. Cu and Ru increase slightly the value of this intercept in Figure 3b, suggesting an increase in the probability of oxygen removal *via* reactions with CO.

The catalytic properties of Fe-Zn-K_2, Fe-Zn-K_2-Cu_1, and Fe-Zn-K_2-Ru_1 are compared in Table 1 at similar CO conversion levels. The addition of Cu or Ru to Fe-Zn oxide precursors led to two-fold and four-fold increases in hydrocarbon synthesis rates, respectively. These promotion effects cannot be explained by the FTS activity of the Ru promoter, which even if atomically dispersed would account for only about 20% of the rate increase observed upon Ru addition, using reported FTS turnover rates on Ru/SiO_2 (16). C_{5+} formation rates increased proportionately with the observed increase in hydrocarbon synthesis rates, leading to nearly identical selectivities on all catalysts. The slightly lighter products formed on Cu- and Ru-promoted samples reflect the lower surface density of the potassium promoter for the higher surface areas prevalent in metal-promoted samples, as discussed below. Ru, and to a lesser extent Cu, appear to increase the number of FTS active sites formed during the activation of Fe-Zn oxide precursors. This proposal is confirmed below by measurements of the structural evolution of the active phases during reaction and by surface area and CO chemisorption measurements after catalyst activation during Fischer-Tropsch synthesis.

Surface Areas and CO Chemisorption Site Densities on Fresh and Activated Fe-Zn-K-Cu(Ru) Oxides

Table 2 shows BET surface areas and CO chemisorption uptakes on Fe-Zn-K_2, Fe-Zn-K_2-Cu_1, and Fe-Zn-K_2-Ru_1 oxide precursors after FTS reactions for 1 h at the conditions indicated in the caption. BET surface areas are also reported for the oxide precursors after thermal treatment in air at 673 K for 4 h, but before FTS reactions. Before reaction, BET surface areas were mostly unaffected by the presence of Cu or Ru promoters. After FTS reactions for 1 h, surface areas

were higher on the metal-promoted samples than on unpromoted samples, suggesting that smaller crystallites of Fe_3O_4 and FeC_x formed when Cu or Ru was present during *in situ* activation of Fe-Zn oxide precursors.

CO chemisorption uptakes on activated samples were significantly higher when Cu or Ru was present, suggesting the formation of more CO adsorption sites when Fe-Zn oxide precursors were activated in the presence of Cu or Ru reduction-carburization promoters. Chemisorption uptakes were higher on the Ru-promoted sample than for the sample modified by Cu, a trend also observed for hydrocarbon synthesis rates. This apparent correlation between FTS rates and CO chemisorption uptakes was also observed for Zn-free Fe-K-Cu sample (4). It is consistent with Cu and Ru favoring the formation of smaller Fe carbide crystallites, which in turn provide a higher density of sites for CO chemisorption and for FTS reaction turnovers. Thus, it appears that these reduction-carburization promoters increase the rate of catalyst activation by providing a large number of nucleation sites, which favor the formation of smaller FeC_x and Fe_3O_4 crystallites. These smaller crystallites and the faster carburization kinetics introduced by Cu and Ru were probed directly during activation of Fe-Zn oxide precursors using *in situ* X-ray absorption spectroscopy, as described in the next section.

Structural Characterization of Fe-Zn-K-Cu(Ru) Catalysts During Fischer-Tropsch Synthesis Using X-Ray Absorption Spectroscopy

In situ Fe K-edge X-ray absorption spectroscopy was used to monitor the structural evolution of Fe-Zn oxides during activation and FTS reactions, and the effects of Cu and Ru on the relative abundance and kinetics of the structures formed as Fe-Zn oxide precursors undergo activation during contact with synthesis gas at FTS conditions. Fe_2O_3, Fe_3O_4, and FeC_x were identified by principal component analysis methods and the sample spectra were fitted as linear combinations of these standard compounds as a function of time in contact with synthesis gas. FeC_x concentrations are reported as Fe atomic fractions as a function of contact time in Figure 4. The reduction and carburization rates and the extent of carburization of these materials are smaller than for the Zn-free samples reported previously (4), because Zn species, in the form of $ZnFe_2O_4$, inhibit the rate of reduction/carburization processes (5). The structure evolves, however, in a manner similar to that reported previously for these Zn-free samples - *via* the initial formation of Fe_3O_4 and the rapid subsequent transformation of this phase into FeC_x (4). Since the details of such transformations are very similar for Fe and Fe-Zn oxide precursors, we restrict our discussion here to the extent and kinetics of FeC_x formation and to the effect of Cu and Ru on these properties on Fe-Zn oxide precursors.

Figure 4 shows that Cu, and especially Ru, increased carburization rates and the steady-state extent of carburization of Fe-Zn oxide precursors promoted also with K. The faster carburization kinetics with synthesis gas confirm the promoting effect reported above using either H_2 or CO as the reducing agents. As shown in Figure 4, the extent of carburization is also higher on samples promoted with Ru or Cu than on the Fe-Zn-K sample. The FeC_x content, however, reached an almost constant value after ~8 h on stream at the conditions of this study (Figure 4). Thus, while faster carburization may lead to the faster attainment of steady-state FTS reaction rates, it should not lead to higher steady-state FTS reaction rates, which are measured after contact with synthesis gas for more than 24 h. Also, it is not obvious how the greater extent of carburization achieved, when Cu or Ru is present, would lead to higher steady-state FTS rates, because

previous studies on promoted Fe_2O_3 precursors have shown that the carburization of only a few near-surface layers is sufficient for steady-state FTS reaction rates (17). We conclude that the extent of carburization is controlled by the diffusion path for the removal of lattice oxygen from the core of Fe oxide precursors. Thus, the shorter diffusion path in the smaller crystallites formed on promoted samples during activation is responsible for the greater extent of carburization on the promoted samples. In this manner, both the higher FTS rates and the faster and more extensive carburization find a common cause in the role of promoters in promoting the nucleation of the Fe active phase as smaller crystallites. No causal relationship between the extent of carburization and the observed FTS reaction rates is warranted by these observations.

Isothermal Transient Analysis of Reduction, Carburization, and Fischer-Tropsch Synthesis Products during Activation of Fe-Zn-K-Cu(Ru) Catalysts

Fischer-Tropsch synthesis rates were measured during exposure to synthesis gas at the same conditions as those used in X-ray absorption experiments ($H_2/CO=2$, 523 K) in order to relate the observed structural evolution to the rate of hydrocarbon formation as Fe oxide catalyst precursors activate during FTS. CH_4 formation rates measured on Fe-Zn-K oxide precursors promoted with Cu or Ru are shown in Figure 5 as a function of time. For unpromoted Fe-Zn-K oxides, a short induction period was observed upon initial contact with synthesis gas. CH_4 was immediately detected, however, on Fe-Zn oxides promoted with Cu or Ru. CH_4 formation rates during the initial stages and at steady state were higher on promoted than on unpromoted catalysts. The initial increase in CH_4 formation rates is accompanied in all samples by the formation of an excess amount of CO_2 and H_2O, indicative of the removal of lattice oxygen during the reduction and carburization of the oxide precursors. These reduction-carburization processes are faster on the Ru-containing samples than on the Cu-containing or unpromoted Fe-Zn-K samples. Steady state FTS rates were attained after ~1 h in contact with synthesis gas, even though X-ray absorption spectra detected a continuing increase in FeC_x content up to ~ 8 h. These data confirm the previous proposal that FTS reactions are influenced only by the density of active carbide sites in near-surface layers, irrespective of a remaining Fe oxide core (17). These data are also consistent with the FTS data at higher pressures reported above and with a role of Cu or Ru in favoring the formation of smaller and more easily carburized structures from Fe-Zn-K oxide precursors.

On samples containing Cu or Ru (Table 2), FTS rates increased proportionally with the observed increase in FeC_x content and in CO chemisorption uptakes. All these results clearly show that Cu and Ru favor the formation of more dispersed active phases, and that chemical promotion effects, such as an increase in the turnover rate of FeC_x sites, are unnecessary in order to account for the observed increase in FTS rates when Cu or Ru is present during the activation of Fe-Zn oxide precursors. These conclusions, along with the previous observation that higher surface area precursors prepared by incorporating ZnO during the precipitation of Fe_2O_3 also led to higher FTS reaction rates (6), led us to attempt the synthesis of more highly dispersed active carbide phases by using Fe oxide precursors with higher surface areas, as we report in the next section.

Synthesis of Fe-Zn-K-Cu Oxides Precursors with High Surface Area

Our efforts to improve the dispersion and site density of the FeC_x structures formed during reaction included the development of synthetic methods to increase the surface area of Fe-Zn oxide precursors and to minimize the sintering that occurs during drying and impregnation with Cu(Ru) and K. In this section, we examine promoter concentrations required in order to optimize catalysts prepared from precursors with varying surface area. We also establish the surface density of the Cu and K promoters (~2 atom/nm^2 for K and 1 atom/nm^2 for Cu), instead of atomic content, as the relevant controlling variable in determining the dispersion and catalytic properties of FeC_x structures.

Several factors, such as the drying processes after precipitation or impregnation and the temperature and time of thermal treatments designed to decompose precursors influence the surface area of the Fe-Zn oxide precursors. These factors were systematically examined in order to increase catalyst surface area and improve FTS catalytic performance. The effect of precipitation pH was examined previously; it was found that a pH of 7.0 held constant during precipitation led to the highest precursor surface areas (18). The effect of Zn/Fe ratio on the performance of Fe-Zn-K catalysts for FTS reactions was also previously studied and a Zn/Fe atomic ratio of 0.1 was found to give highest FTS reaction rates (19).

Sintering of porous materials often occurs because of pore pinching during the final stages of drying, even at low temperatures. This process is particularly important for water, because of its high surface tension (γ=72 mN/m at 298 K). Alcohols have much lower surface tensions (e.g. γ=22 mN/m for ethanol and isopropanol at 298 K) and they are also known to act as surface-active agents that decrease the surface tension of aqueous solutions (20). Therefore, the water contained within the pores in Fe-Zn oxide precipitates was replaced before drying by extensive washing with either ethanol or isopropanol in an attempt to inhibit sintering of Fe-Zn oxide precursors during drying.

Figure 6 shows the surface area of Fe-Zn oxide precursors with different intrapore liquids after thermal treatment at various temperatures (Figure 6a-c). After drying at 398 K for 12 h, ethanol or isopropanol-washed precipitates showed much higher Fe-Zn oxyhydroxide surface areas than precipitates dried without replacing intrapore water with alcohols (215 vs. 148 m^2/g). The similar precursor surface areas obtained with isopropanol and ethanol are consistent with their similar surface energies. All other precipitation variables were kept constant; therefore, it appears that the drying step and the surface tension of the intrapore liquids during drying strongly influenced the pore structure and the surface area of the Fe-Zn oxide precursors. Our data show that a high space velocity of dry air (~2000 cm^3/h.g-cat.) is required in order to minimize sintering during hydroxide decomposition. The replacement of H_2O with lower surface tension liquids during the drying process and the rapid removal of H_2O as it forms during hydroxide decomposition at higher temperatures are critical variables in preserving the initial surface area of the precipitated precursors.

The temperature and time of the final thermal treatment in air also influenced Fe-Zn oxide surface areas. After drying oxyhydroxide precipitates with different intrapore liquids at 398 K for 12 h, they were treated in flowing dry air at various temperatures for 4 h in order to establish

optimum treatment protocols. All samples showed the expected decrease in surface area with increasing treatment temperature, but the higher surface area samples obtained by drying alcohol-containing precipitates were more sensitive to the treatment temperature. X-ray diffraction confirmed that Fe-Zn hydroxides formed poorly crystalline Fe_2O_3 at ~543 K. Zn, possibly as the $ZnFe_2O_4$ phase detected in samples with higher Zn/Fe ratio (>0.2) and treated at higher temperatures (~673 K), was well dispersed and not detected in these alcohol-washed samples. It appears that thermal treatment at 543 K provides a compromise between structural purity and a high surface area in Fe_2O_3, and that the surface area of the resulting oxide is highest when intrapore water is replaced with lower surface tension liquids, such as alcohols.

The effects of impregnation with K and Cu promoters on surface areas were also investigated. Fe-Zn oxyhydroxide precursors were impregnated with K carbonate (K/Fe=0.02) and dried at 393 K for 12 h. Ru nitrosyl nitrate (Ru/Fe=0.01) was then added as Ru nitrosyl nitrate *via* similar impregnation procedures. The addition of K to Fe-Zn hydroxide precursors decreased its surface area (220 vs. 192 m^2/g), apparently because of the collapse of the pores induced by the removal of high surface tension intrapore liquids. Similarly, the subsequent impregnation of the Fe-Zn-K with Ru led to an additional decrease in its surface area. Each impregnation and subsequent drying decreased the surface area by 10-20%. Ru-promoted Fe-Zn-K hydroxides were then treated at different temperatures in order to examine the effect of treatment temperature on the surface areas (Figure 4d). Here, the effects of temperature on the surface area of promoted Fe-Zn-K-Ru oxides were similar to that on the Fe-Zn oxides. The surface area of Ru-promoted Fe-Zn-K oxides decreased from 142 to 96 m^2/g as thermal treatment temperatures increased from 523 to 623 K**.**

Based on these surface areas for Fe-Zn hydroxides and Fe-Zn-K-Ru oxide precursors prepared by different methods, we selected a procedure for maximizing the surface area of Fe-Zn-K-Cu samples. Fe-Zn hydroxide precursors were first prepared by co-precipitation at a constant pH of 7.0 and the precipitates were thoroughly washed with ethanol in order to replace intrapore water. Fe-Zn hydroxide precursors were then treated at 543 K for 4 h in flowing dry air at 2000 cm^3/h.g-cat. The resulting Fe-Zn oxide precursors were impregnated with K and Cu using incipient wetness impregnation method and aqueous solutions of Cu nitrate and K carbonate. The amounts of K (K/Fe=0.04) and Cu (Cu/Fe=0.02) were chosen so as to maintain the K and Cu surface densities at the values previously shown to maximize FTS reaction rates on conventionally prepared samples (~2 K-atom/nm^2; 1 Cu-atom/nm^2). The surface area of the resulting Fe-Zn-K_4-Cu_2 oxides was 120 m^2/g, almost twice that of the Fe-Zn-K_2-Cu_1 oxide samples. As a result, the K and Cu content were chosen to be about twice as high as that on the conventionally prepared Fe-Zn-K_2-Cu_1 sample. A sample prepared from high surface area Fe-Zn oxide precursors led to lower FTS rates and significantly lighter products than the sample with the higher promoter concentrations (Fe-Zn-K_4-Cu_2), suggesting the presence of sub-optimum levels of K and Cu and confirming the relevant role of atomic surface density as the defining variable in the design of these promoted catalytic materials.

Site Density of Active Species and Promoters and Effects on the Fischer-Tropsch Synthesis

The relevance of these improvements in surface area to the performance of these materials in FTS reactions was confirmed by the FTS rate and selectivity measurements on a high surface area Fe-Zn-K_4-Cu_2 oxide (120 m^2/g) and on a lower surface area Fe-Zn-K_2-Cu_1 oxide prepared

via conventional methods (65 m^2/g). The amounts of K and Cu in the Fe-Zn-K_4-Cu_2 sample were chosen so as to maintain the same surface density of promoters as in the Fe-Zn-K_2-Cu_1 sample prepared from Fe-Zn oxide precursors with lower surface area. Steady state FTS rates and selectivities at 508 K and 2.14 MPa are shown as a function of CO conversion for these two samples in Figure 7. Hydrocarbon synthesis rates are about two-fold higher on Fe-Zn-K_4-Cu_2 than on Fe-Zn-K_2-Cu_1, a difference that corresponds to the difference in the surface areas of their respective Fe-Zn oxide precursors. The similarities between these two samples in CO_2 and C_{5+} selectivities, in α-olefin/*n*-paraffin ratios, and in their kinetic response of FTS rates to changes in conversion, suggest that the synthetic protocols used to increase the precursor surface areas led to a larger number of active sites in working catalysts, without any detectable changes in chain growth pathways.

Figure 8 shows FeC_x concentrations obtained from XAS measurements of the structural evolution of these oxide precursors during FTS reactions. Figure 9 shows the corresponding CH_4 formation rates on these two samples at the same conditions used for the X-ray absorption experiments. Both the extent of carbide formation and the CH_4 formation rate at steady state are significantly higher on Fe-Zn-K_4-Cu_2 than on Fe-Zn-K_2-Cu_1 sample. The consistent correlation between the Fe carbide concentration and FTS rates is again not causal, but it confirms that promoters (Ru, Cu, K) and higher surface area precursors increase the density of active sites in the Fe carbide structures prevalent during steady-state Fischer-Tropsch synthesis. Accordingly, we examine next whether further increases in the surface density of these promoters leads to additional improvements in active site density and in FTS rates. We prepared a Fe-Zn-K-Cu samples using the same Fe-Zn oxide precursor and treated the sample at the same conditions as the Fe-Zn-K_2-Cu_1 sample but with a higher K concentration (Fe-Zn-K_4-Cu_1).

Table 3 compares FTS performance, surface area, CO chemisorption uptake, and the extent of carburization for Fe-Zn-K_2-Cu_1, and Fe-Zn-K_4-Cu_1 and Fe-Zn-K_4-Cu_2 catalysts. Fe-Zn-K_2-Cu_1 and Fe-Zn-K_4-Cu_1 samples have similar surface areas, different potassium contents and surface densities (2 vs. 4 atom/nm^2); yet, similar FTS reaction rates, CO chemisorption uptakes, and extents of carburization were obtained. This suggests that the higher K surface density did not lead to an additional increase in the number of active sites, possibly because excess K leads to larger promoter domains without significantly improved contact between the promoter and the Fe oxide precursors or a higher actual density of K species. We have observed that increasing Cu or K concentrations beyond those required to achieve surface densities of 2 and 4 atom/nm^2, respectively, do not increase FTS reaction rates. Fe-Zn-K_2-Cu_1 and Fe-Zn-K_4-Cu_2 samples have different BET surface areas but similar apparent surface densities of K and Cu on the available surface area. The Fe-Zn-K_4-Cu_2 sample with the higher surface area shows higher FTS rates and a higher density of CO binding sites, indicating that higher precursor surface areas lead to proportionately higher FTS rates and active site densities, as long as the promoter surface densities are kept above a threshold value. These results suggest that promoter concentrations are more appropriately defined in terms of surface density in designing catalysts with similar and optimum promoter contents as the surface areas of the Fe oxide precursors are changed by modifying precipitation, drying, and promoter impregnation methods. The consistent agreement between the increase of FTS rates and the increase in surface area, CO adsorption site availability, and the concentration of Fe carbides suggests that higher FTS activity can be achieved by the design and appropriate promotion of high surface area oxide precursors.

Fischer-Tropsch Synthesis Rates and Selectivities on Fe-Zn-K_4-Cu_2 and Co/SiO_2 Catalysts

The apparent low FTS activity of Fe-based catalysts at conditions normally employed for Co-based FTS catalysts (473 K-488 K) has led to their predominant use at significantly higher temperatures (500 K-543 K) than Co catalysts. In this section, we provide a comparison between the performances of the Fe-Zn-K_4-Cu_2 catalyst with that of the best Fe-based catalysts reported in the literature at similar reaction conditions. Then, we show that the high FTS rates attained on high surface area Fe-Zn-K_4-Cu_2 catalysts allow their use at conditions typical of Co-based catalysts (473 K, 2 MPa, H_2/CO=2). At these conditions, Fe-Zn-K_4-Cu_2 shows hydrocarbon synthesis productivities similar to those observed on Co/SiO_2 catalysts.

A comparison of Fe-Zn-K_4-Cu_2 samples with previously reported Fe-based catalysts (at H_2/CO=~1.7-2.0) is shown in Table 4 at relatively high CO conversions (~50%). The results from low-surface area Fe-Zn-K_2-Cu_1 are representative of the catalyst reported in reference (6). Fe-Zn- K_4-Cu_2 gives nearly twice the CO conversion rate and hydrocarbon synthesis productivity of a commercial Ruhrchemie AG catalyst (Fe-SiO_2-$K_{5.9}$-$Cu_{4.4}$) (21), and nearly three times that of the Fe-Zn-K_2-Cu_1 catalyst, even though our Fe-Zn-K_4-Cu_2 catalysts were tested at lower temperatures (508 K vs. 523-543 K). Fe-Zn-K_4-Cu_2 also compares well with a Fe-$Si_{4.6}$-$K_{1.4}$ catalyst tested at 543 K (22, 23). CO_2 selectivities are lower on Fe-Zn-K_4-Cu_2 than on the other catalysts, apparently as a result of the lower operating temperatures made possible by its high FTS activity. The proper design of synthesis, promotion, and activation protocols that increase the density of active sites available for FTS reactions have led to further increases in hydrocarbon synthesis productivities, even after several decades of active research on Fe-based FTS catalysts.

The high surface area Fe-Zn-K_4-Cu_2 sample was also compared with a Co/SiO_2 catalyst at 473 K and 2 MPa, conditions typical of Co-based FTS catalysts. Fe-based catalysts must generally be operated at significantly higher temperatures, because of their lower catalytic activity. It is worth noting that Co-based catalysts can be operated only within a very narrow range of temperatures (473-500 K), pressure (~2 MPa), and synthesis gas stoichiometry (H_2/CO=~2), because of their predominant methanation activity at higher temperatures, lower pressures, and higher H_2/CO ratios.

Hydrocarbon productivities, CH_4 selectivities, C_{5+} selectivities, *1*-pentene/*n*-pentane ratios and *1*-decene/*n*-decane ratios are shown as a function of CO conversion for Fe-Zn-K_4-Cu_2 and Co/SiO_2 in Figures 10a-e. Table 5 provides a summary of these comparisons at similar CO conversions (18-21%). Hydrocarbon synthesis productivities are very similar on these two catalysts (Table 5, Figure 10a). Hydrocarbon synthesis turnover rates estimated from the number of sites available on the Co (from H_2 chemisorption before reaction) and the Fe (from CO chemisorption after reaction) catalysts are higher on Co (60.9 h^{-1}) than on Fe (19.8 h^{-1}) at identical reaction conditions (Table 5). Reaction rates increased slightly with CO conversion on Co catalysts, because of a promoting effect of water on FTS reaction rates (10). CH_4 selectivities (Figure 10b) were significantly lower on Fe than on Co catalysts, but C_{5+} selectivities (Figure 10c) were very similar on the two catalysts because of higher C_2-C_4 olefin selectivities on Fe (Fe: 6.4%; Co: 4.4%). The *1*-pentene/*n*-pentane ratios are similar on the two catalysts (Figure 10d and Table 5).

Larger hydrocarbons are essentially paraffinic on Co catalysts (2) because of significant readsorption and chain initiation by α-olefins formed in primary chain termination steps, as shown by the *1*-decene/n-decane ratios on Co than on Fe catalysts (Figure 10e, Table 5).

In summary, hydrocarbon synthesis rates on Fe-Zn-K_4-Cu_2 prepared *via* the synthesis, promotion, and activation protocols reported here are nearly identical to those on Co/SiO_2 catalysts representative of the state-of-the-art. The lower apparent turnover rates on Fe-based catalysts are compensated by the larger density of active sites per gram of catalyst on these Fe catalysts to yield similar hydrocarbon synthesis rates per gram of catalyst. These Fe-based catalysts, with their lower CH_4 selectivities and more olefinic products, provide attractive alternatives to Co-based catalysts. Their higher CO_2 selectivity, even at low temperatures, continues to disfavor their use for natural gas-derived synthesis gas mixtures. Additional decreases in CO_2 selectivities on Fe catalysts will require a further decrease in reaction temperatures or the internal recycle of some CO_2 to the inlet of the FTS reactor or to the synthesis gas generation unit. These Fe-based catalysts also show a much weaker selectivity dependence on temperature, pressure, and synthesis gas ratio than Co catalysts.

Conclusions

High FTS activity can be achieved by the design and appropriate promotion of high surface area oxide precursors. The presence of Cu or Ru in the Fe-Zn-K oxide matrix significantly increased the rates for the reduction and carburization of Fe-Zn oxide precursors, by promoting the nucleation of reduced Fe species (Fe_3O_4, FeC_x), and leading to the formation of smaller FeC_x crystallites. As indicated by the markedly increased steady-state FTS rates without any concurrent changes in product selectivities, these smaller FeC_x crystallites formed in aid of promoters provide a larger number of active sites for FTS reactions. The consistent agreement between the increase of FTS rates and the increase in surface area, CO adsorption site availability, and the concentration of Fe carbides on these Cu- and Ru-promoted Fe-Zn oxide samples suggests that the effect of promoters is to provide a higher density of active sites by forming smaller FeC_x crystallites. However, increasing the atomic concentrations of K and/or Cu without concurrently increasing the surface area of Fe-Zn precursors did not necessarily lead to higher surface promoter density required for the promotion of active site density for an increased FTS rate. Accordingly, a K- and Cu-promoted high surface area Fe-Zn oxide catalyst has been synthesized by an appropriate choice of the solvent used in the drying step of the catalyst preparation and a proper introduction of promoters. A significantly improved FTS performance has been achieved. The performance of this Fe-Zn-Cu-K catalyst exhibits hydrocarbon productivities similar to that of Co catalysts at conditions typically employed for Co-FTS.

Acknowledgements

This work was supported by the U. S. Department of Energy (DOE) under contract number DE-FC26-98FT40308. X-ray absorption data were collected at the Stanford Synchrotron Radiation Laboratory (SSRL), which is operated by the Department of Energy (DOE), Office of Basic Energy Sciences under contract DE-ACO3-76SF00515. The authors thank Mr. Bjorn Moden, Mr. Dario Pinna, and Dr. Patrick DaCosta for their assistance with the acquisition of the X-ray absorption data.

References

1. Dry, M. E., The Fisher-Tropsch Synthesis, in *Catalysis-Science and Technology*, Vol. 1, p. 160. J. R. Anderson and M. Boudart eds., Springer Verlag, New York, 1981.
2. Brady, R. C., and Pettit, R., *J. Am. Chem. Soc*. **103**, 1287 (1981).
3. Schulz, H., *Appl. Catal. A* **186**, 3 (1999).
4. Li, S., Meitzner, G. D., and Iglesia, E., *J. Phys. Chem. in press*.
5. Li, S., Li, A., Krishnamoorthy, S., and Iglesia, E., *submitted to Appl. Catal*.
6. Soled, S. L., Iglesia, E., Miseo, S., DeRites, B. A., and Fiato, R. A., *Topics in Catal.* **2**, 193 (1995).
7. Habermehl, R., and Atwood, K., *Am. Chem. Soc. Div. Fuel. Chem. Prepr*., **8**, 10 (1964).
8. Vannice, M. A., *J. Catal*. **37**, 462 (1975).
9. Iglesia, E., Soled, S. L., Fiato, R. A., and Via, G. H., *J. Catal*. **143**, 345 (1993).
10. Iglesia, E., *Appl. Catal. A* **161**, 59 (1997).
11. Iglesia, E., Soled, S. L., Baumgartner, J. E., and Reyes, S. C., *J. Catal.* **153**, 108 (1995).
12. Amelse, J. A., Butt, J. B., and Schwartz, L. H., *J. Phys. Chem. B* **82**, 558 (1978).
13. WinXAS97 is an XAS data analysis program for PCs running MS-Windows by Thorsten Ressler (http://ourworld.compuserve.com/homepages/t_ressler).
14. Malinowski, E. R., Howery, D. G., in *Factor Analysis in Chemistry,* John Wiley & Sons: New York, 1981.
15. Meitzner, G. D., and Huang, E. S., *Fresenius J. Anal. Chem.* **342**, 61 (1992).
16. Madon, R. J., and Iglesia, E., *J. Catal.* **139**, 576 (1993)
17. Li, S., Meitzner. G. D., and Iglesia, E., *submitted to J. Catal.*
18. Soled, S. L., and Iglesia, E., *unpublished results.*
19. Li, A., Li, S., and Iglesia, E., *unpublished results.*
20. Lide, D. R., and Frederikse, H. P. R., Ed.; *Handbook of Chemistry and Physics*, 75th Ed.; The Chemical Rubber Company press: Boca Raton, 1994.
21. Van der Laan, G. P., and Beenackers, A. A. C. M., *Ind. Eng. Chem. Res.* **38**, 1277 (1999).
22. Raje, A. P., and Davis, B. H., *Catal. Today* **36**, 335 (1997).
23. Raje, A. P., O'Brien, R., and Davis, B. H., *J. Catal.* **180**, 36 (1998).

Table 1. Steady-state Fischer-Tropsch synthesis rates and selectivities on Fe-Zn-K_2, Fe-Zn-K_2-Cu_1, and Fe-Zn-K_2-Ru_1 samples (atomic ratios: Zn/Fe=0.1, K/Fe=0.02, Cu(Ru)/Fe=0.01; H_2/CO=2, 508 K, 2.14 Mpa, CO conversion is13-16%).

Sample	Fe-Zn-K_2	Fe-Zn-K_2-Cu_1	Fe-Zn-K_2-Ru_1
CO conversion rate (mol CO/h.g-atFe)	1.7	3.5	7.2
CO_2 formation rate (mol CO/h.g-at.Fe)	0.2	0.7	1.1
Hydrocarbon formation rate (mol CO/h.g-at.Fe)	1.5	2.8	6.0
CO_2 selectivity (%)	11.5	20.2	16.8
CH_4 selectivity (%)[a]	2.0	2.4	2.8
C_{5+} selectivity (%)[a]	88.2	85.3	85.0
1-C_5H_{10}/*n*-C_5H_{12} ratio	2.3	2.5	2.5

[a]CH_4 and C_{5+} selectivities are reported on a CO_2-free basis.

Table 2. BET surface areas and CO chemisorption uptakes on Fe-Zn-K_2, Fe-Zn-K_2-Cu_1, and Fe-Zn-K_2-Ru_1 samples after FTS reactions (H_2/CO=2, 523 K, 1 h); Fe carbide concentrations were obtained from *in situ* XAS measurements; CH_4 formation rates were obtained from isothermal transient experiments.

Sample	Fe-Zn-K_2	Fe-Zn-K_2-Cu_1	Fe-Zn-K_2-Ru_1
Surface area before FTS (m^2/g)	56	65	63
Surface area after FTS[a] (m^2/g)	23	31	39
Amount of CO_x desorbed before CO chemisorption (mmol/g-at. Fe)	11.3	65.3	68.4
Amount of CO_x desorbed after CO chemisorption (mmol/g-at. Fe)	31.6	109.9	124.5
Amount of CO chemisorbed (mmol CO/g-at.Fe)	20.3	44.6	58.1
FeC_x concentration[b] (atom %)	11.8	23.6	57.1
CH_4 formation rate[c] (mmol/s.g-at.Fe)	0.173	0.262	0.372

[a]Surface areas measured after exposure to synthesis gas at 523 K for 1 h (0.2 g sample, K/Fe=0.02, Cu/Fe=0.01, H_2/CO=2, synthesis gas flow rate=64.3 mol/h.g-at.Fe

[b]FeC_x concentration measured after exposure to synthesis gas at 523 K for 5 h (1 mg precipitated Fe_2O_3, K/Fe=0.02, Cu/Fe=0.01, H_2/CO=2, synthesis gas flow rate=107 mol/h g-at.Fe).

[c]CH_4 formation rates measured after exposure to synthesis gas at 523 K for 1 h (0.2 g sample, K/Fe=0.02, Cu/Fe=0.01, H_2/CO=2, synthesis gas flow rate=64.3 mol/h.g-at.Fe).

Table 3. Steady state FTS rates and selectivities ($H_2/CO=2$, 508 K, 2.140 Mpa, CO conversion is 13-16%), and the characterization results for Fe-Zn-K_2-Cu_1, Fe-Zn-K_4-Cu_1 and Fe-Zn-K_4-Cu_2 samples after FTS reactions.

Sample	Fe-Zn-K_2-Cu_1	Fe-Zn-K_4-Cu_1	Fe-Zn-K_4-Cu_2
CO conversion rate (mol CO/h.g-at.Fe)	3.5	3.6	6.8
CO_2 formation rate (mol CO/h.g-at.Fe)	0.7	0.8	1.4
Hydrocarbon formation rate (mol CO/h.g-at.Fe)	2.8	2.8	5.4
CO_2 selectivity (%)	20.2	22.4	20.5
CH_4 selectivity (%)[a]	2.4	2.4	3.8
C_{5+} selectivity (%)[a]	85.3	85.5	80.8
1-C_5H_{10}/*n*-C_5H_{12} ratio	2.5	2.5	2.7
Surface area before FTS (m^2/g)	65	58	120
Surface area after FTS[b] (m^2/g)	31	26	43
Amount of CO_x desorbed before CO chemisorption (mmol/g-at.Fe)	65.3	72.0	75.2
Amount of CO_x desorbed after CO chemisorption (mmol/g-at.Fe)	109.9	112.3	141.1
Amount of CO chemisorbed (mmol CO/g-at.Fe)	44.6	40.3	65.9
FeC_x concentration[c] (atom %)	23.6	-	69.2
CH_4 formation rate[d] (mmol/s.g-at.Fe)	0.262	0.289	0.527

[a]CH_4 and C_{5+} selectivities are reported on a CO_2-free basis.
[b]Surface areas measured after exposure to synthesis gas at 523 K for 1 h (0.2 g sample, K/Fe=0.02, Cu/Fe=0.01, $H_2/CO=2$, synthesis gas flow rate=64.3 mol/h g-at. Fe
[c]FeC_x concentration measured after exposure to synthesis gas at 523 K for 5 h (1 mg precipitated Fe_2O_3, K/Fe=0.02, Cu/Fe=0.01, $H_2/CO=2$, synthesis gas flow rate=107 mol/h g-at. Fe).
[d]CH_4 formation rates measured after exposure to synthesis gas at 523 K for 1 h (0.2 g sample, K/Fe=0.02, Cu/Fe=0.01, $H_2/CO=2$, synthesis gas flow rate=64.3 mol/h g-at. Fe).

Table 4. Steady-state FTS performance of various Fe-based catalysts using natural gas-derived synthesis gas (H_2/CO=1.7-2.0)

Catalyst	Fe-Zn-K_4-Cu_2 (this work)	Fe-Zn-K_2-Cu_1 (this work)	Fe-$Si_{4.6}$-$K_{1.4}$(22,23)	Fe-SiO_2-$K_{5.9}$-$Cu_{4.4}$ [Ruhrchemie LP33/81] (21)
Reactor Type	Fixed-Bed	Slurry	Slurry	Spinning Basket
Temperature (K)	508	543	543	523
Pressure (MPa)	2.14	0.50	1.31	2.40
H_2/CO ratio	2.0	2.0	1.7	2.0
CO space velocity (NL/h.g-cat)	3.4	1.4	5.7	2.4*
CO conversion (%)	50.8	55.5	50.0*	52.7
CO rate (mol CO/h.g-cat)	0.08	0.03	0.12*	0.05*
Hydrocarbon productivity (g/h.kg.cat)	765	258	1008*	404
CO_2 selectivity (%)	31.7	48.6	40.0*	42.3*

*- Values calculated based on reported data or graphs

Table 5. A comparison of the steady state FT performances between Fe and Co catalysts (473 K, 2 MPa, $H_2/CO=2$) at CO conversion range of 18~21% (atomic ratios: Zn/Fe=0.1, K/Fe=0.04, Cu/Fe=0.02; 21.9 wt.% Co/SiO_2).

Catalyst	Fe-Zn-K_4-Cu_2	Co/SiO_2
Total available metal sites for FTS ($\times 10^{-4}$ mol/g.cat.)	7.4	1.7
Hydrocarbon synthesis turnover rate (h^{-1})	16.7	59.6
Hydrocarbon productivity (g/h/kg.cat.)	171	143
CO_2 selectivity (%)	15.8	0.3
CH_4 (%)[a]	2.0	6.8
C_2-C_4 (%)[a]	8.9	6.4
C_{5+} (%)[a]	89.1	86.8
1-C_5H_{10}/*n*-C_5H_{12} ratio	2.1	2.0
1-$C_{10}H_{20}$/*n*-$C_{10}H_{22}$ ratio	1.6	0.3

[a] CH_4 and C_{5+} selectivities are reported on a CO_2-free basis.

Figure 1. Oxygen removal rates for Fe-Zn-K-Cu(Ru) oxides in H_2. (a) Fe-Zn-K_2 sample, (b) Fe-Zn-K_2-Cu_1 sample, (c) Fe-Zn-K_2-Ru_1 sample. (0.2 g sample; K/Fe=0.02, Cu(Ru)/Fe=0.01; 0.167 K/s ramping rate; 20% H_2/Ar, 0.268 mol/h flow rate)

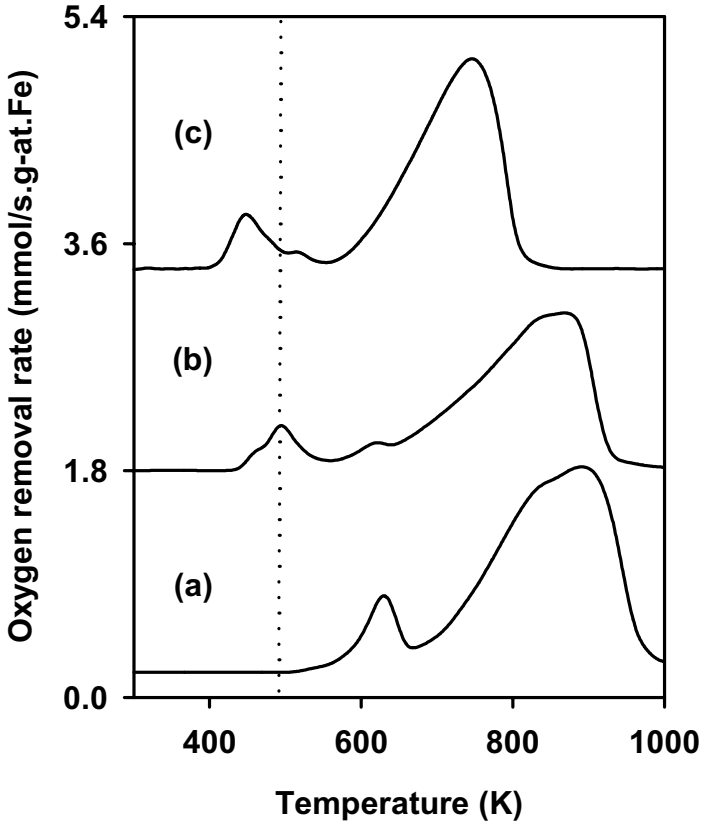

Figure 2. Oxygen removal and carbon introduction rates for Fe-Zn-K-Cu(Ru) samples in CO. (a) Fe-Zn-K_2 sample, (b) Fe-Zn-K_2-Cu_1 sample, (c) Fe-Zn-K_2-Ru_1 sample. (0.05 g sample; K/Fe=0.02, Cu(Ru)/Fe=0.01; 0.167 K/s ramping rate; 20% CO/Ar, 0.268 mol/h flow rate)

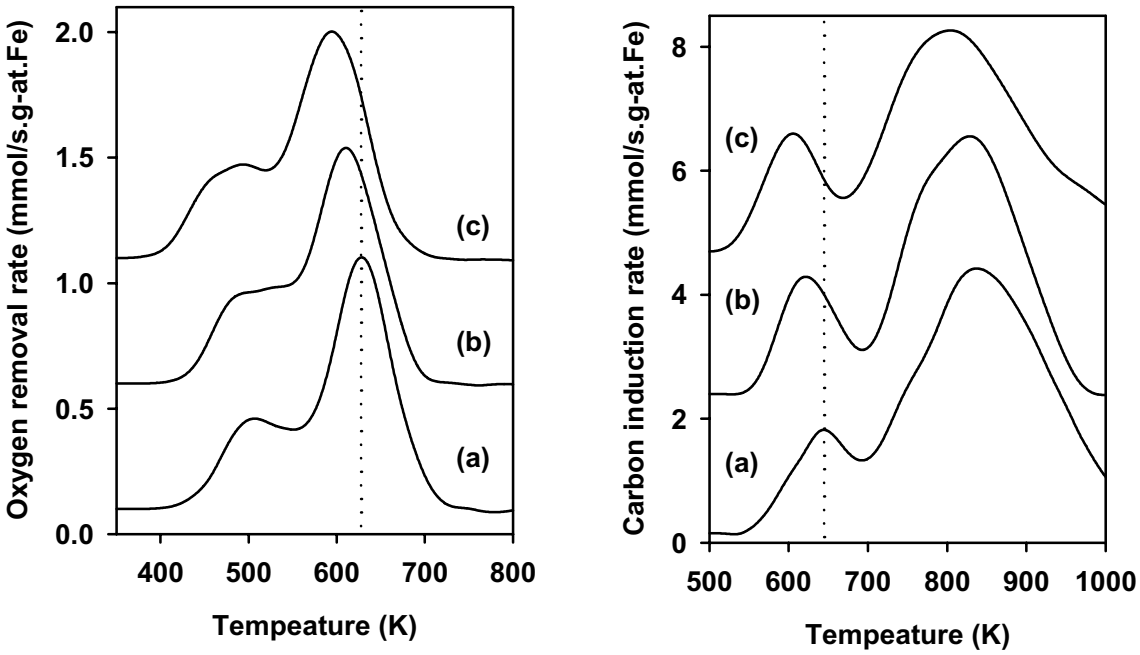

Figure 3. Steady-state FTS rates and selectivities on promoted Fe oxide catalysts as a function of CO conversion (H_2/CO=2, 508 K and 2.14 MPa). (a) Hydrocarbon synthesis rate, (b) CO_2 selectivity, (c) C_{5+} selectivity, and (d) *1*-C_5H_{10}/*n*-C_5/H_{12} ratio. (■) Fe-Zn-K_2 oxide, (●) Fe-Zn-K_2-Cu_1 oxide, and (◆) Fe-Zn-K_2-Ru_1 oxide.

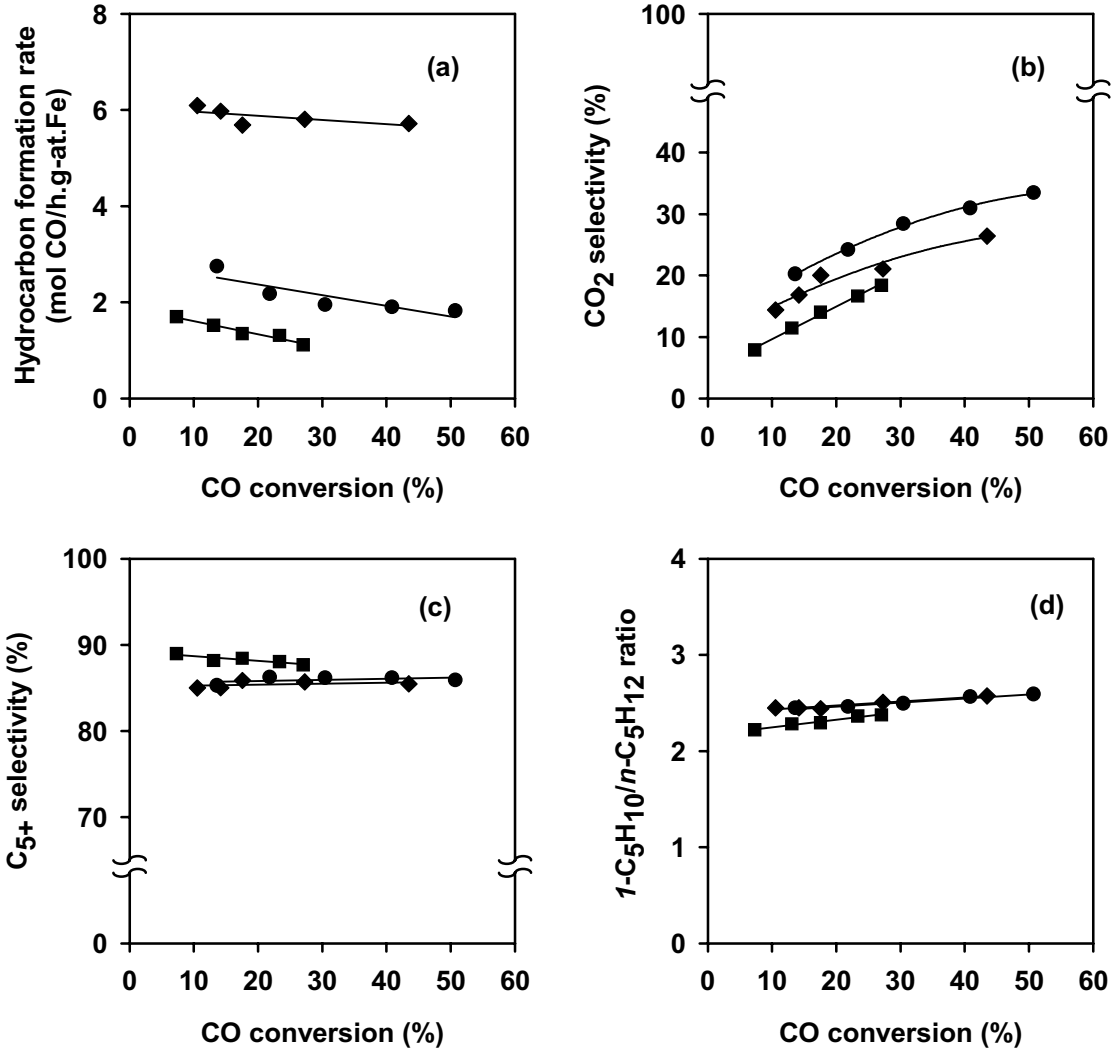

Figure 4. The evolution of Fe carbides during *in situ* XAS measurement of Fe-Zn-K-Cu(Ru) samples in synthesis gas. (a) Fe-Zn-K_2 sample, (b) Fe-Zn-K_2-Cu_1 sample, (c) Fe-Zn-K_2-Ru_1 sample. (1 mg sample, K/Fe=0.02, Cu(Ru)/Fe=0.01, H_2/CO=2, synthesis gas flow rate=107 mol/h.g-at.Fe)

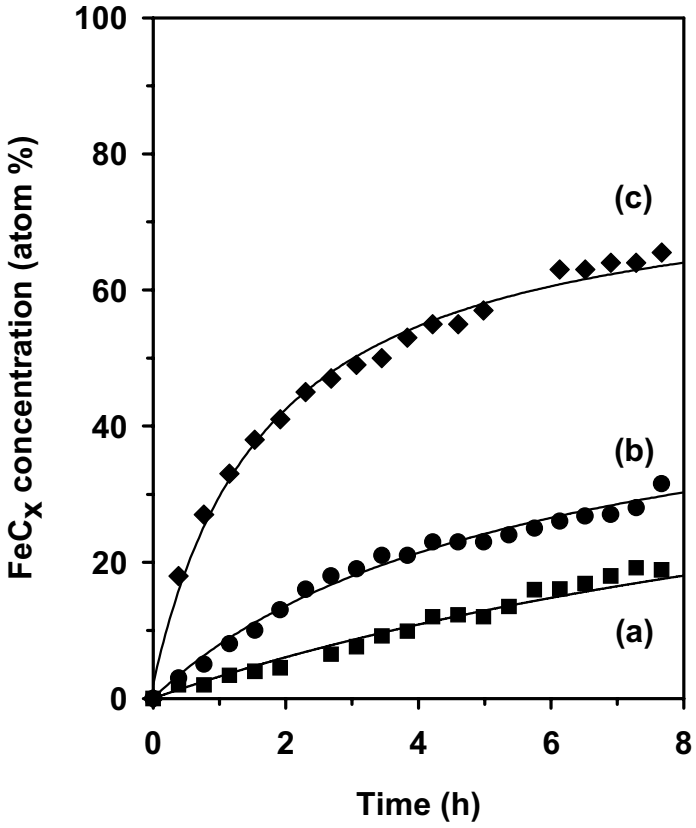

Figure 5. CH_4 formation rate as a function of reaction time in contact with synthesis gas ($H_2/CO=2$, 523 K, synthesis gas flow rate=107 mol/h.g-at.Fe). (a) Fe-Zn-K_2 sample, (b) Fe-Zn-K_2-Cu_1 sample, (c) Fe-Zn-K_2-Ru_1 sample.

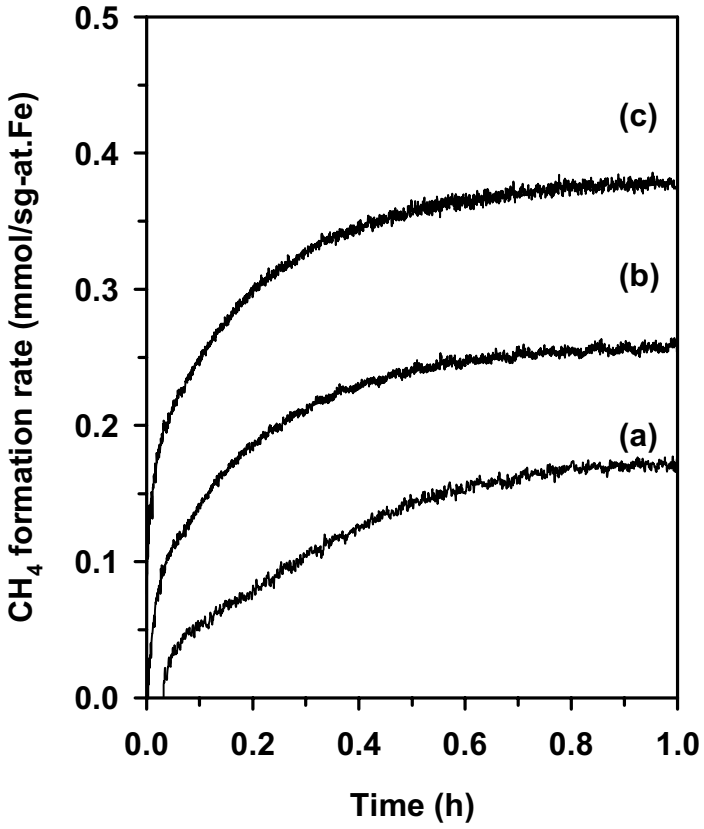

Figure 6. BET surface areas of Fe-Zn and Fe-Zn-K_2-Ru_1 samples dried with various intrapore liquids as a function of thermal treatment temperature. (a) Fe-Zn precursor washed by intrapore water (■), (b) Fe-Zn precursor washed by intrapore ethanol (●), (c) Fe-Zn precursor washed by intrapore isopropanol (+), (d) Fe-Zn precursor washed by ethanol and subsequently promoted with K and Ru (◆) (K/Fe=0.02, Ru/Fe=0.01). (All the samples were treated in dry air at the stated temperature for 4 h).

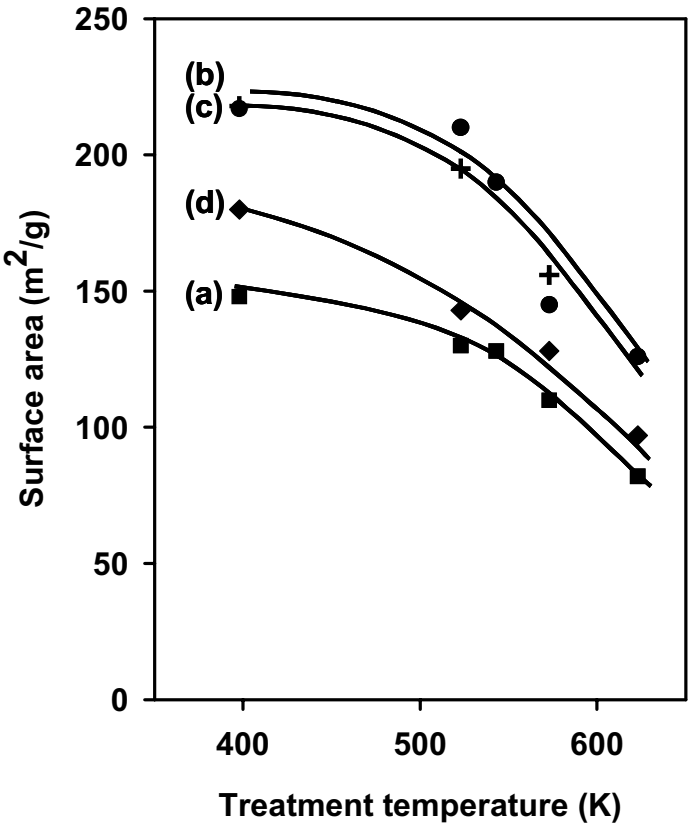

Figure 7. Comparison of the FTS activity of (●) Fe-Zn-K_2-Cu_1 sample, and (▲) Fe-Zn-K_4-Cu_2 sample as a function of CO conversion at steady-state reaction conditions (H_2/CO=2, 508 K and 2.14 MPa). (a) Hydrocarbon formation rate, (b) CO_2 selectivity, (c) C_{5+} selectivity, and (d) *1*-C_5H_{10}/*n*-C_5/H_{12} ratio.

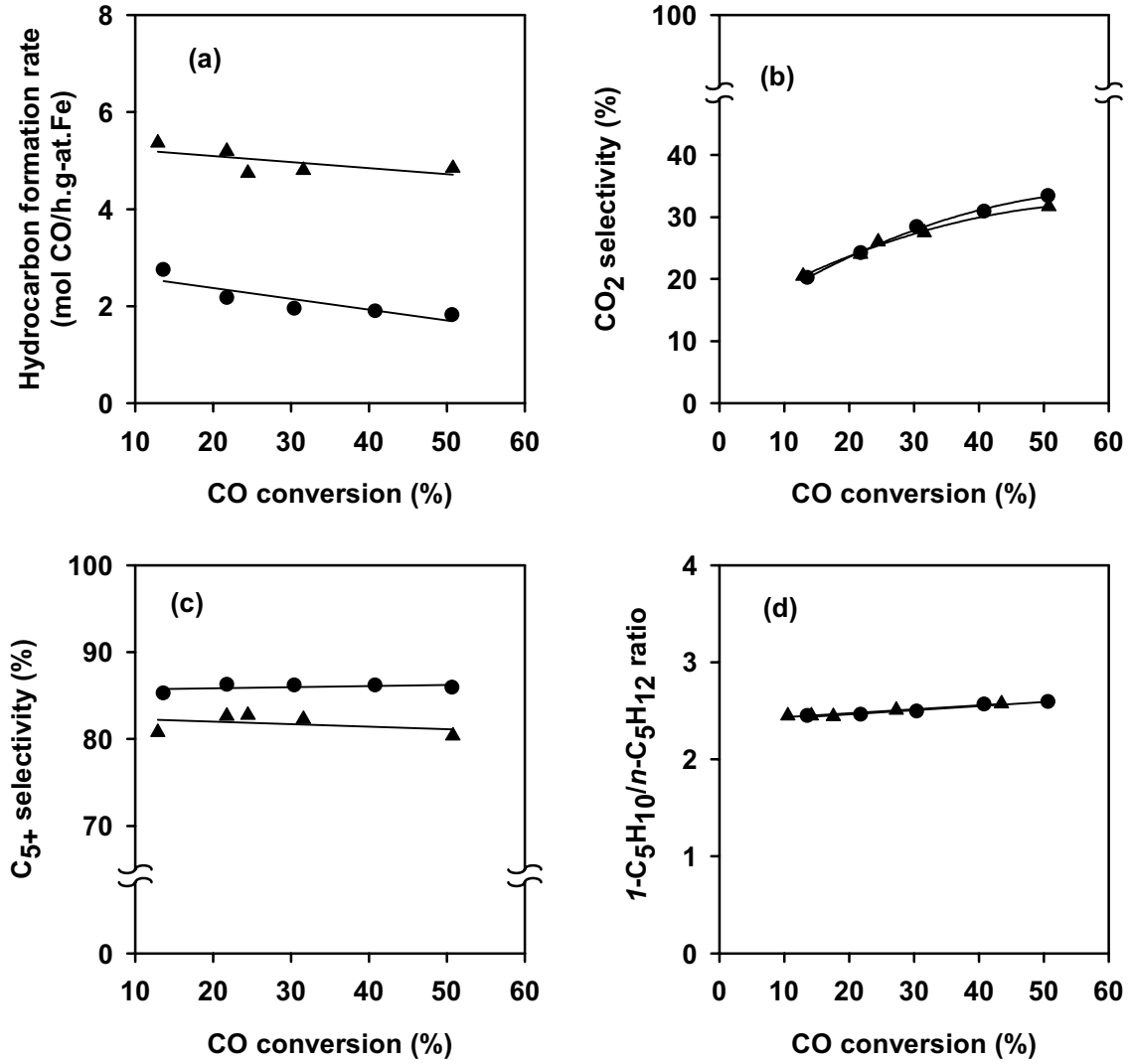

Figure 8. FeC_x concentrations as a function of time on (a) Fe-Zn-K_2-Cu_1 and (b) Fe-Zn-K_4-Cu_2 samples as a function of reaction time during *in situ* X-ray absorption measurements in synthesis gas (1 mg precipitated sample, $H_2/CO=2$, synthesis gas flow rate=107 mol/h.g-at.Fe)

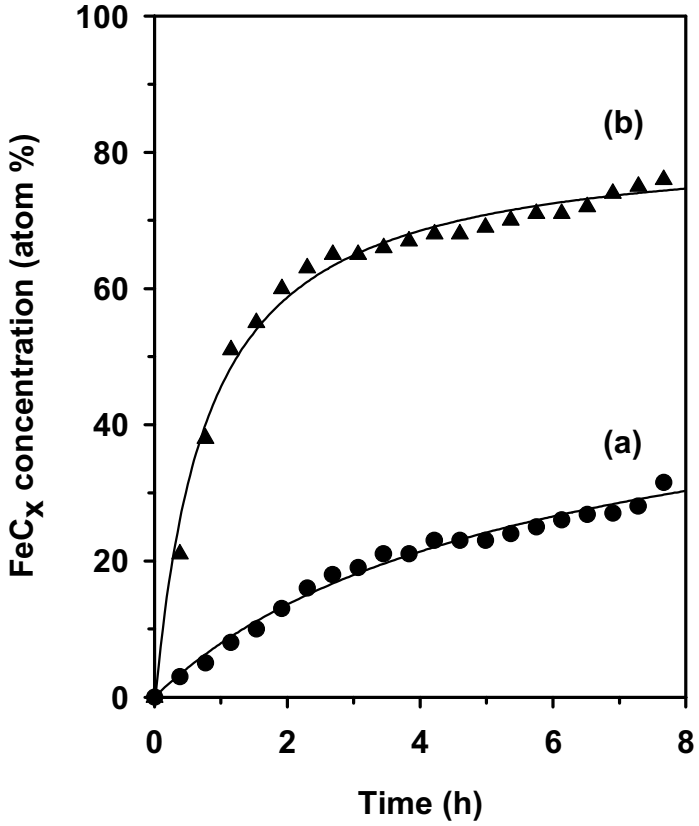

Figure 9. CH_4 formation rates as a function of time in contact with synthesis gas at the conditions of X-ray absorption measurements shown in Figure 8 ($H_2/CO=2$, 523 K, synthesis gas flow rate=107 mol/h.g-at.Fe). (a) Fe-Zn-K_2-Cu_1 sample, (b) Fe-Zn-K_4-Cu_2 sample.

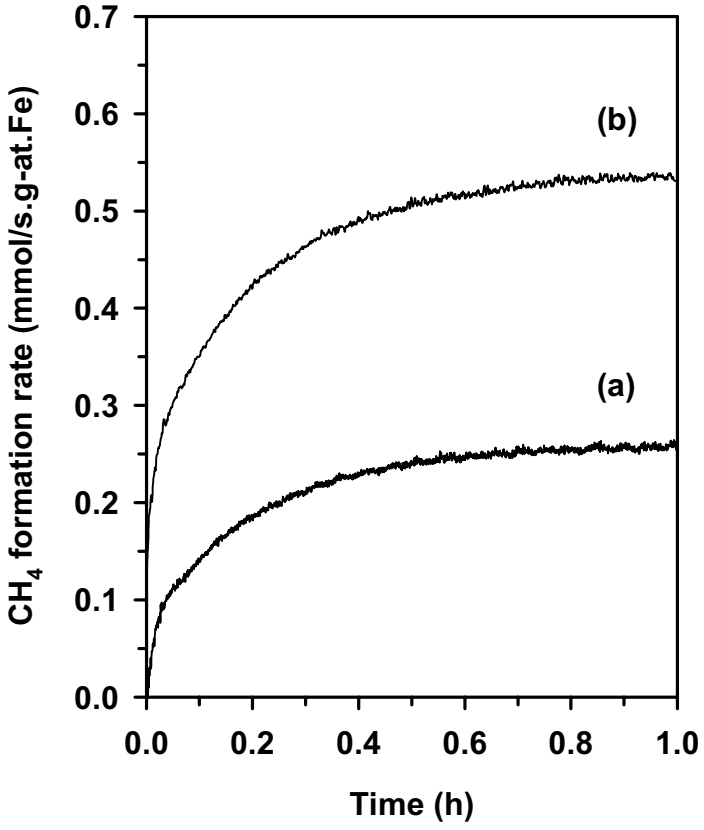

Figure 10. Comparison of the performance of the Fe-Zn-K_4-Cu_2 (●) and a 21.9 wt.% Co/SiO_2 (■) catalysts for the FTS reactions (473 K and 2.14 MPa, H_2/CO=2).). (a) Hydrocarbon productivity, (b) CO_2 selectivity, (c) C_{5+} selectivity, and (d) *1*-C_5H_{10}/*n*-C_5H_{12} ratio, and (d) *1*-$C_{10}H_{20}$/*n*-C_{10}/H_{22} ratio.

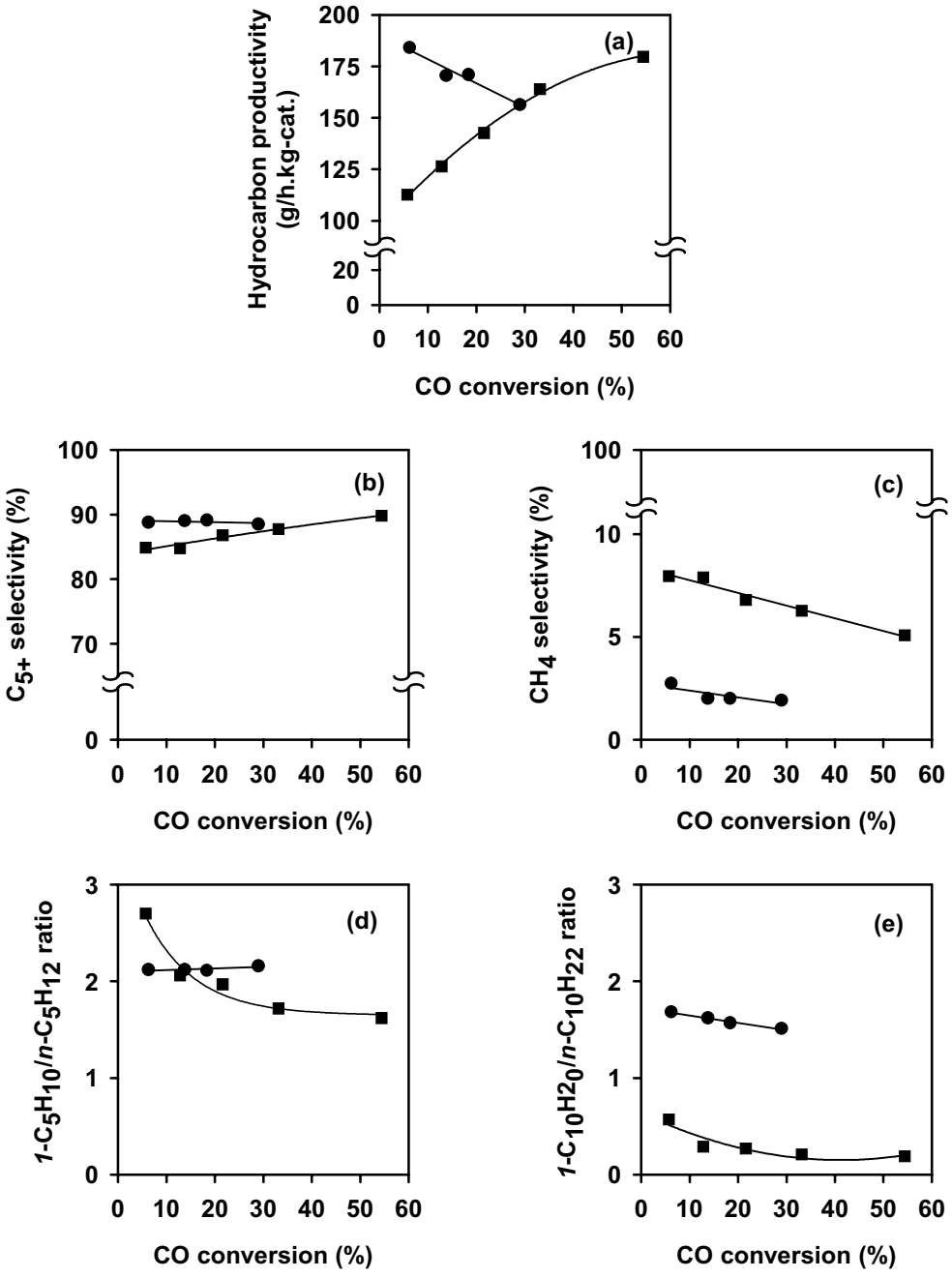

5. FISCHER-TROPSCH SYNTHESIS ON FE-BASED CATALYSTS

5.1 Effect of H_2/CO ratio on the performance of Fe-Zn-Cu-K for FTS

FTS experiments were conducted with the high activity Fe-Zn-Cu_2-K_4 catalyst at 473 K, P_{CO}=150 kPa and varying H_2/CO ratios. These experiments were conducted in order to provide better understanding of the behavior of Fe catalysts under varying H*/CO* surface coverages as well as probing possible similarities in chain growth behavior on Fe and Co catalysts under similar H*/CO* coverages. Experiments were conducted at H_2/CO ratios of 2, 10 and 20.

The CO rates at the three conditions are compared as a function of CO conversion in Figure 5.1. The rate increases with hydrogen surface coverage on the catalyst indicating a positive dependence of observed FTS rates on hydrogen partial pressures. The CO rate at 473 K and 500 kPa (H_2/CO=2) is lower than that at 473 K and 2000 kPa reported earlier (0.45 and 1.35 mol/h.mol Fe at ~20% conversion) [25]. This effect is expected from the lower concentrations of H_2 and CO at the lower pressure. Also, the CO_2 selectivity curves shown in Figure 5.2 indicate the possibility of an unchanged y-intercept (determined by the primary mode of CO_2 formation) and a smaller slope, indicative of water gas-shift rates, with increase in H* surface coverage. Thus an increase in H* surface concentration impacts the extent of removal of O* as H_2O instead of CO_2. This decrease in CO_2 formed *via* the secondary water-gas shift reaction is as a result of a corresponding increase in the reverse rate of the reaction, i.e., between CO_2 and H_2. In our previous experiments conducted at 508 K and 543 K on the Fe catalysts, the water-gas shift reaction does not approach equilibrium until high conversions at 543 K [18-21].

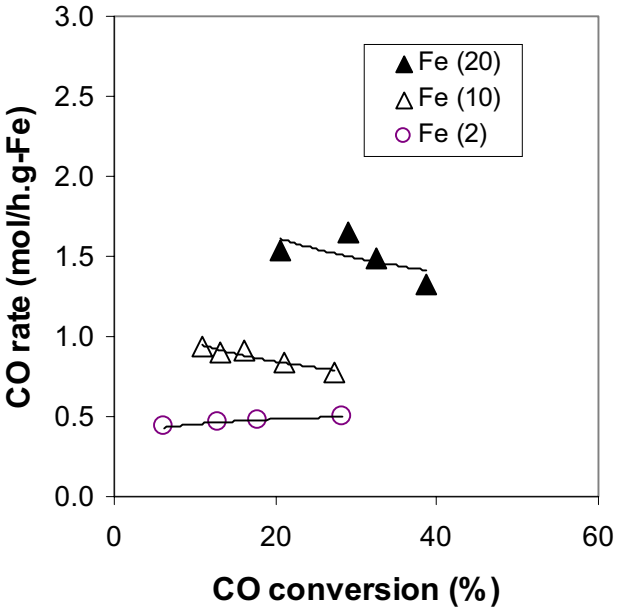

Figure 5.1 CO conversion rate as a function of CO conversion on Fe-Zn-Cu-K (Zn/Fe=0.1, Cu/M=0.02, K/M=0.04), at different H_2/CO ratios, 473 K, P_{CO}=150 kPa.

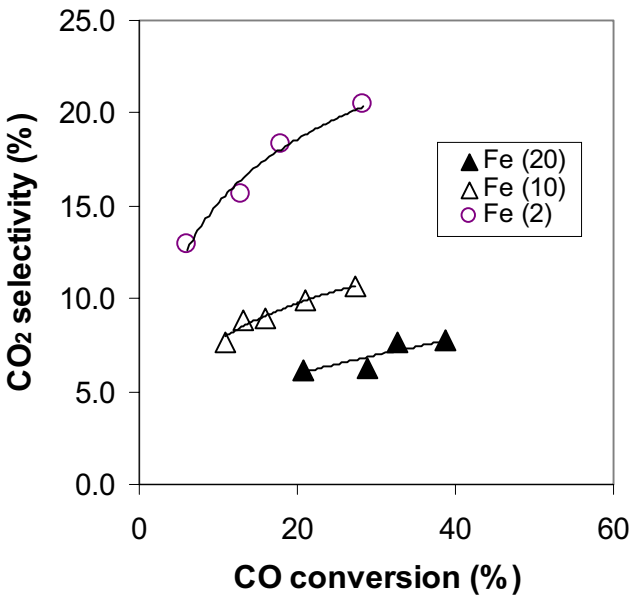

Figure 5.2 CO_2 selectivity as a function of CO conversion on Fe-Zn-Cu-K (Zn/Fe=0.1, Cu/M=0.02, K/M=0.04), at different H_2/CO ratios, 473 K, P_{CO}=150 kPa.

The water gas-shift reaction equilibrium constant (K) is approximately 60 at 543 K and 200 at 473 K. However with an increase in H_2 partial pressure by a factor of 5 and 10, the reaction is much closer to equilibrium as observed with η, which is the extent of the water gas-shift reaction towards equilibrium, given by

$$\eta = \frac{\left(\frac{P_{CO_2} P_{H_2}}{P_{CO} P_{H_2}} \right)}{K}$$

shown as a function of conversion in Figure 5.3.

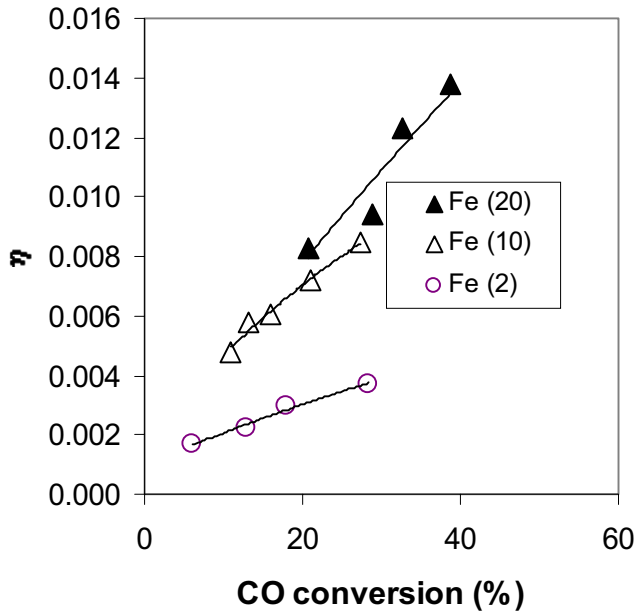

Figure 5.3. η, the extent of the water gas equilibrium towards equilibirum as a function of CO conversion on Fe-Zn-Cu-K (Zn/Fe=0.1, Cu/M=0.02, K/M=0.04), at different H_2/CO ratios, 473 K, P_{CO}=150 kPa.

The surface H* availability also affects the CH_4 selectivity in the product distribution (Figure 5.4. Upon increasing the H_2/CO ratio from 2 to 10 to 20, the CH_4 selectivity increased from 1.2% to 4.4% to 6.8%. The C_{5+} selectivity (Figure 5.5) decreased upon increasing the H* surface concentration, which indicates a tendency of hydrocarbon chains to terminate at lower carbon numbers as H* becomes more abundant near chain growth sites.

In conjunction with these observations, the olefin content in the products decreased with increasing H_2/CO ratios, indicating a great tendency for chains to terminate as paraffins instead of olefins, even for small chains. The α-olefin/*n*-paraffin ratio is shown as a function of carbon number in Figure 5.6. The olefin content decreased with increasing carbon number because heavier olefins diffused more slowly within inside catalyst pores, and have a greater tendency to readsorb and grow until their desorption as unreactive larger paraffins. For the same reason, a

change in olefin content upon increasing H* coverages has a lower impact on the higher molecular weight hydrocarbons.

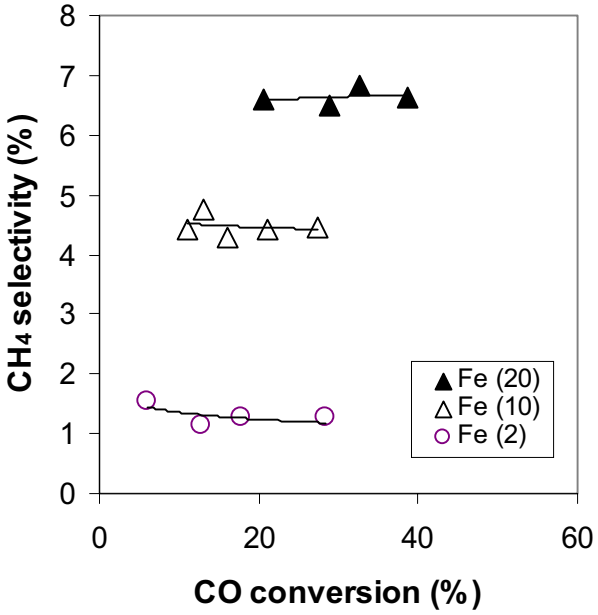

Figure 5.4 CH_4 selectivity (CO_2-free) as a function of CO conversion on Fe-Zn-Cu-K (Zn/Fe=0.1, Cu/M=0.02, K/M=0.04), at different H_2/CO ratios, 473 K, P_{CO}=150 kPa.

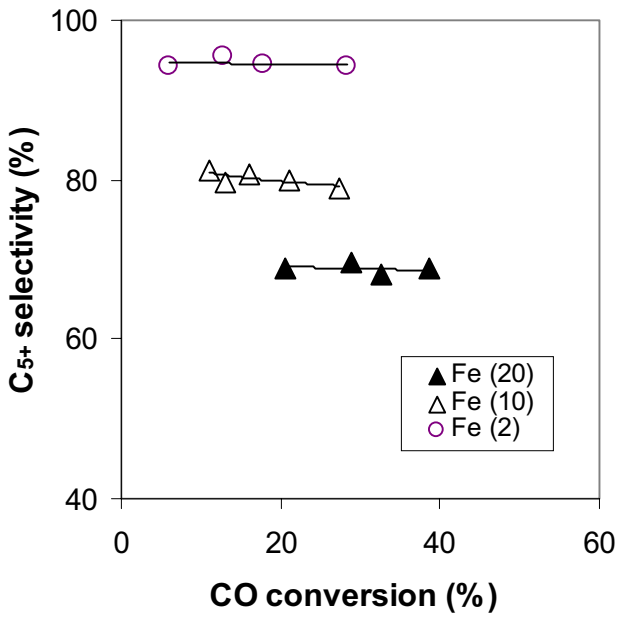

Figure 5.5 C_{5+} selectivity (CO_2-free) as a function of CO conversion on Fe-Zn-Cu-K (Zn/Fe=0.1, Cu/M=0.02, K/M=0.04), at different H_2/CO ratios, 473 K, P_{CO}=150 kPa.

To determine the effect of H* availability on secondary reactions, the *1*-pentene/*1*-pentane ratio is shown as a function of CO conversion in Figure 5.7 at each H_2/CO ratio. At all three conditions, this ratio is independent of CO conversion indicating the absence of secondary reactions such as α-olefin readsorption or hydrogenation, for the low molecular weight hydrocarbons. The high molecular weight α-olefins undergo readsorption on Fe catalysts because of transport restrictions mentioned above, which in turn lead to a curvature in Flory plots at higher carbon numbers.

Because the analysis of wax samples collected at similar conversions at each H_2/CO ratio, has not been completed, a detailed discussion of the effect of H* surface concentration on the chain termination and growth mechanisms is not included. A comparison of the chain growth behavior on Fe catalysts coupled with that for a Co/SiO_2 sample tested at 473 K, 500 kPa and H_2/CO=2, will provide insight on the similarity in behavior between Fe and Co when operated at similar surface H*/CO* coverages. This will be presented in the next quarterly report.

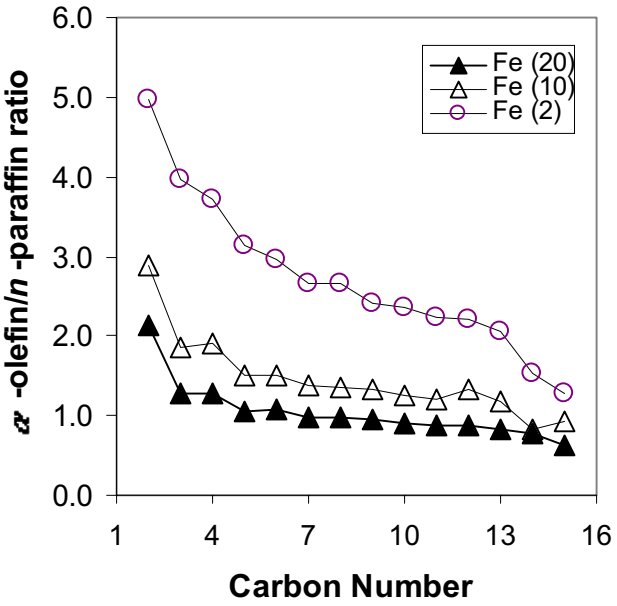

Figure 5.6 α-olefin/*n*-paraffin ratios as a function of carbon number on Fe-Zn-Cu-K (Zn/Fe=0.1, Cu/M=0.02, K/M=0.04), at different H_2/CO ratios, 473 K, P_{CO}=150 kPa and ~20% CO conversion.

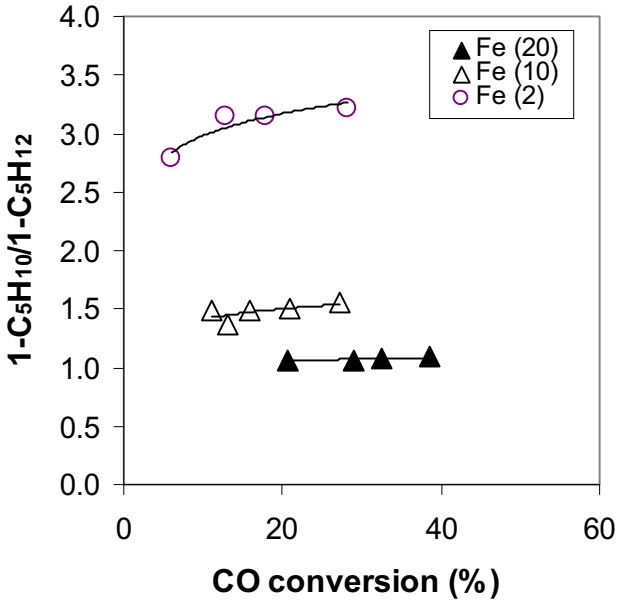

Figure 5.7 *1*-C_5H_{10}/*1*-C_5H_{12} ratio as a function of CO conversion on Fe-Zn-Cu-K (Zn/Fe=0.1, Cu/M=0.02, K/M=0.04), at different H_2/CO ratios, 473 K, P_{CO}=150 kPa.

5.2 FTS reactions on Fe-Zn

During the current reporting period, experiments were also conducted with the low surface area Fe-Zn sample (Zn/Fe=0.1, calcination temperature=673 K), which was used as a precursor for the K- and Cu-promoted catalysts used for FTS reaction experiments reported in earlier quarters [18-21]. This study served to obtain complete picture of the promotion effects of K and Cu on Fe-Zn for FTS.

The CO conversion rate is shown as a function of CO conversion on the different Fe-Zn-based samples at 493 K and 3160 kPa in Figure 5.8. It has previously been observed with our isothermal transient and in situ XAS experiments, that promotion of Fe-Zn by Cu and K, increase the reduction and carburization process of Fe oxides and also increased FT rates [19-22]. Also, the addition of K and Cu caused an effect almost equivalent to a combination of the effects of addition of the individual promoters, which argues against the occurrence of a synergistic effects when promoting with K and Cu [14].

The promotion by Cu and K also increase CO_2 formation rates (Figure 5.9). From the CO_2 selectivity curve it appears that Cu in Fe-Zn mainly promotes primary CO_2 formation without affecting secondary WGS reactions, which is a surprising result considering that Cu is the best reported low temperature WGS catalyst. Promotion by K on the other hand appears to alter the

WGS reaction rather than the primary rate of CO_2 formation. A combination of both K and Cu also increased CO_2 selectivity by increasing the rate of secondary WGS reactions.

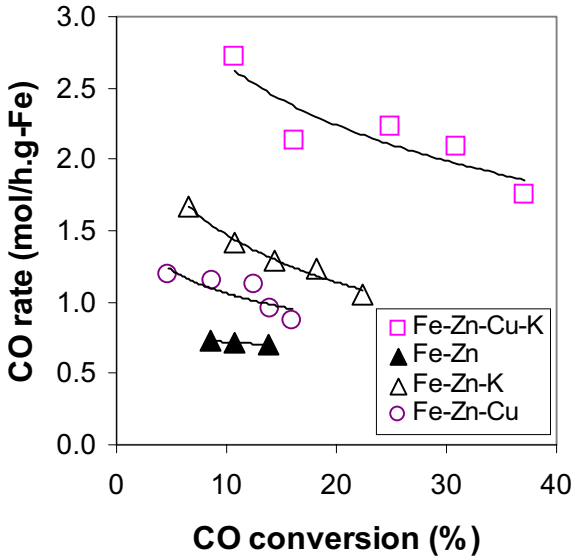

Figure 5.8 CO conversion rate as a function of CO conversion on different Fe-Zn samples at 493 K, 3160 kPa, H_2/CO=2.

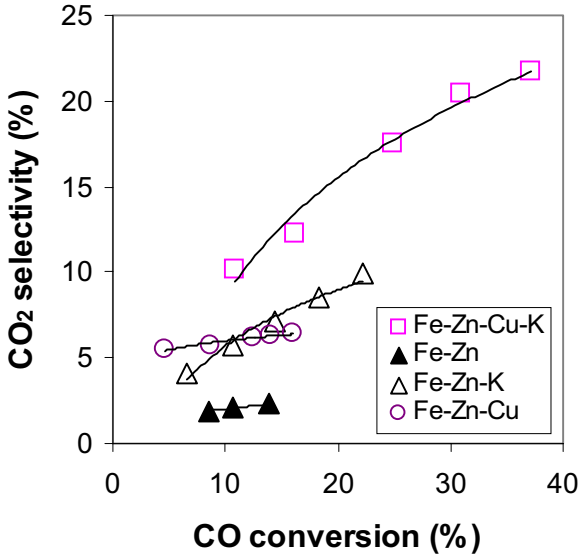

Figure 5.9 CO_2 selectivity as a function of CO conversion on different Fe-Zn samples at 493 K, 3160 kPa, H_2/CO=2.

The product selectivities on different Fe-Zn-based samples are summarized in Table 1. The CH_4 selectivities are highest on the Cu-promoted samples indicating a higher H* availability in the presence of H_2 dissociating sites provided by Cu metal. The K-promoted catalysts have the lowest selectivity to CH_4 irrespective of whether Cu was present or not. This indicates that K decreases H_2 availability on the catalyst. The C_{5+} productivity also increased with K, as a result of a greater tendency for chains to grow rather than hydrogenate when K was present. Secondary reactions, such as isomerization reactions catalyzed by acid sites on the Fe-Zn and Fe-Zn-Cu samples, are eliminated upon promotion with K. The olefin contents, while comparable at C_5, were also much lower at higher carbon numbers (C_{11}) on the samples without K.

Table 1: Hydrocarbon selectivity (CO_2 free) parameters on different Fe-Zn samples at 493 K and 3160 kPa

Catalyst	Fe-Zn	Fe-Zn-Cu	Fe-Zn-K	Fe-Zn-Cu-K
CH_4 (%)	4.8	10.2	1.8	1.8
C_2-C_4 (%)	13.3	17.7	10.7	10.6
C_{5+} (%)	81.9	62.1	87.5	87.6
1-C_5H_{10}/*1*-C_5H_{12} ratio	1.9	1.7	1.8	1.8
1-$C_{11}H_{22}$/*1*-$C_{11}H_{24}$ratio	0.2	0.3	1.5	1.6

Based on these results, the addition of K to Fe-Zn catalysts dramatically inhibit the normal effects of Cu. Even though the loadings of the promoters are in comparable amounts, K appears to decrease the H-dissociating ability of Cu, which is reflected by the sudden decrease in the H* availability. This observation warrants further investigation and will be continued in the upcoming quarter.

II. FISCHER-TROPSCH SYNTHESIS ON COBALT CATALYSTS

1. Transient experiments with Co/SiO_2 catalysts

During the current period, switching experiments were performed after further modifications to the Co-FTS unit were implemented. These modifications were necessary to minimize the dead volume and ensure a good transient response. In particular a new reactor was designed, built and connected to the unit. The response time was calculated as time constant τ (s) using the following model:

$$I(t) = I_1 + (I_2 - I_1) \cdot \left(1 - e^{-\frac{t-t_0}{\tau}} \right) \qquad \text{(II.1)}$$

where t_0 is the time at which the transient begins, $I(t)$ (amp) is the signal at the time t (s), I_1 (amp) is the signal before the switch and I_2 (amp) the signal at the end of the transient. The model (II.1) is representative of a cascade of a continuous stirred reactor and a plug flow reactor.
Preliminary experiments were made at room temperature and high pressure without reaction. In Figure II.1 and II.2 switches from He to H_2 and from CO to H_2, respectively, are reported.

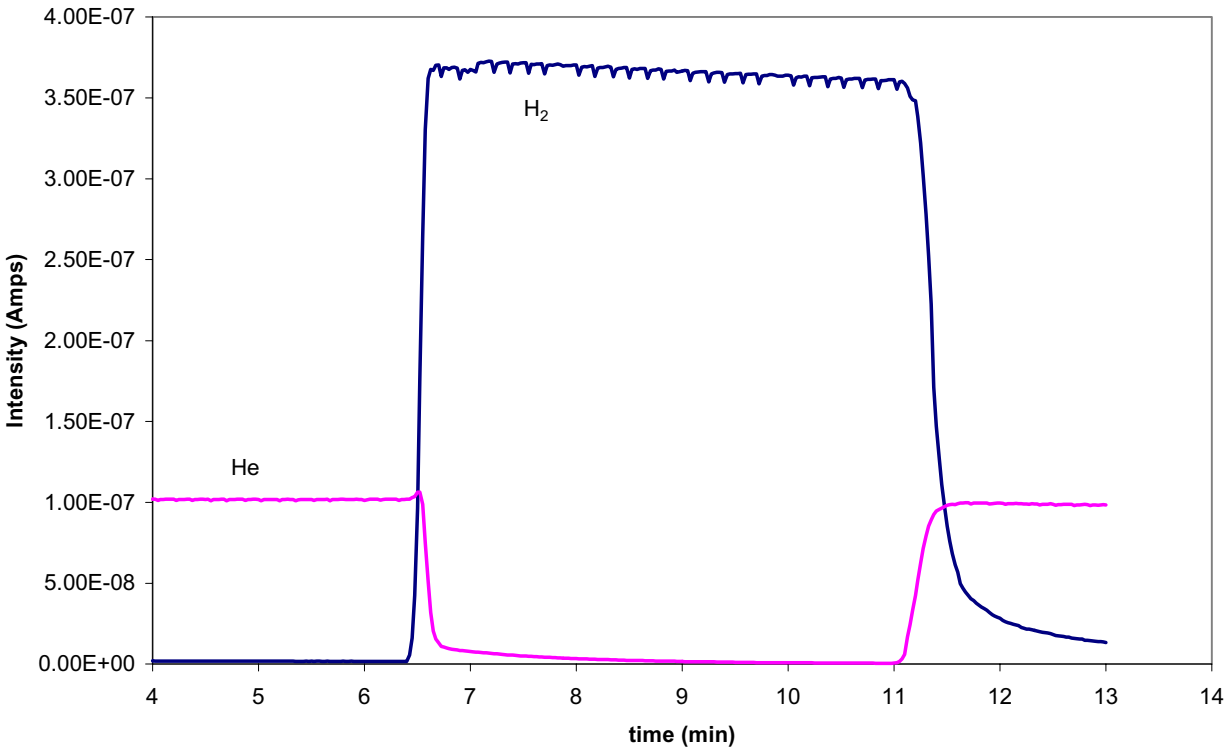

Figure II.1 - Switch from He to H_2 (flow rate = 150 cm^3/min, T = 298 K, P = 650 kPa).

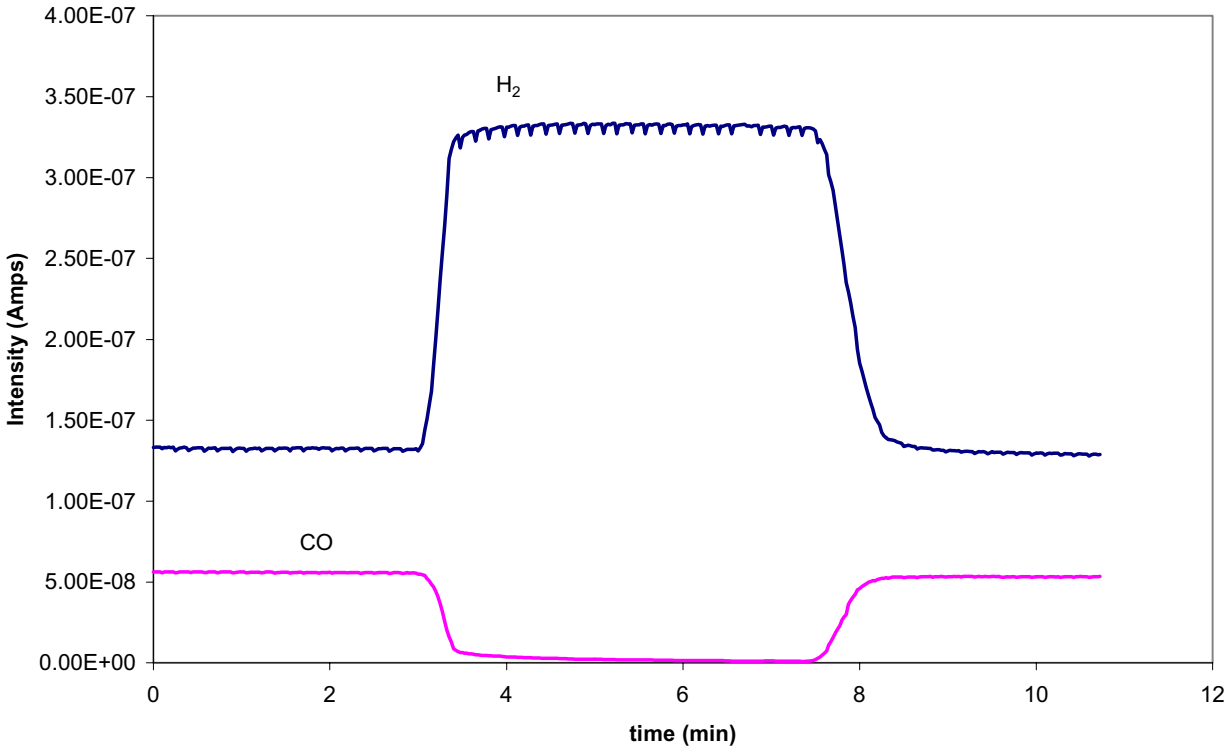

Figure II.2 - Switch from CO to H_2 (flow rate = 100 cm^3/min, T = 298 K, P = 720 kPa)

The values for the time constants were calculated by fitting equation (II.1) to the intensity of the signal of every gas recorded during the transient. The thus calculated values are about 6 s for each gas in both experiments: the reported values for the time constant seems reasonable low.

Therefore further experiments were conducted under FT conditions switching from syngas to hydrogen at high pressure and high temperature. Since the available synthesis gas mixture contained nitrogen as an internal standard (to estimate the CO conversion), it was necessary to introduce another *hydrodynamic internal standard*, in order to monitor the fluid dynamics of the transients. For the experiments presented in this report a known flow rate of He was fed to the reactor, together with the syngas stream, as an internal fluid dynamic standard. In the future a specific mixture of $CO/H_2/Ar$ will be utilized; the higher molecular weight of Ar, in fact, makes its fluid dynamic behaviour more similar to that of CO. The conversion of the electronic signal (intensity) detected by the mass spectrometer into a flow rate was possible by coupling an MS analysis with a GC analysis as follows:

- assuming a linear correlation between the intensity and the flow rate, for each gas detected,
- measuring CO conversion and gaseous product selectivities downstream of the reactor with a GC analysis,
- estimating the flow rates of each gas downstream the reactor from conversion and selectivity

With these premises, the flow rate $F_i(t)$ of the component i at the time t can be calculated from the intensity $I_i(t)$ at the time t with the following relation:

$$F_i(t) = I_i(t) \cdot \left(\frac{F_i^0}{I_i^0} \right) \tag{II.2}$$

where F^{i0} and I^{i0} are the flow rate (cm^3/min) and the intensity (amps) of the component i, respectively, before the switch.

In Figure II.3 we show the results of a switch experiment at T = 465 K, P = 580 kPa, syngas and hydrogen flow rates = 150 cm^3/min. At these conditions the conversion was measured to be about 5% and the methane selectivity about 6% before the switch. The flow rates of the gases shown in the figure were thus estimated as follows: H_2 84 cm^3/min, CO 44 cm^3/min, CH_4 0.12 cm^3/min.

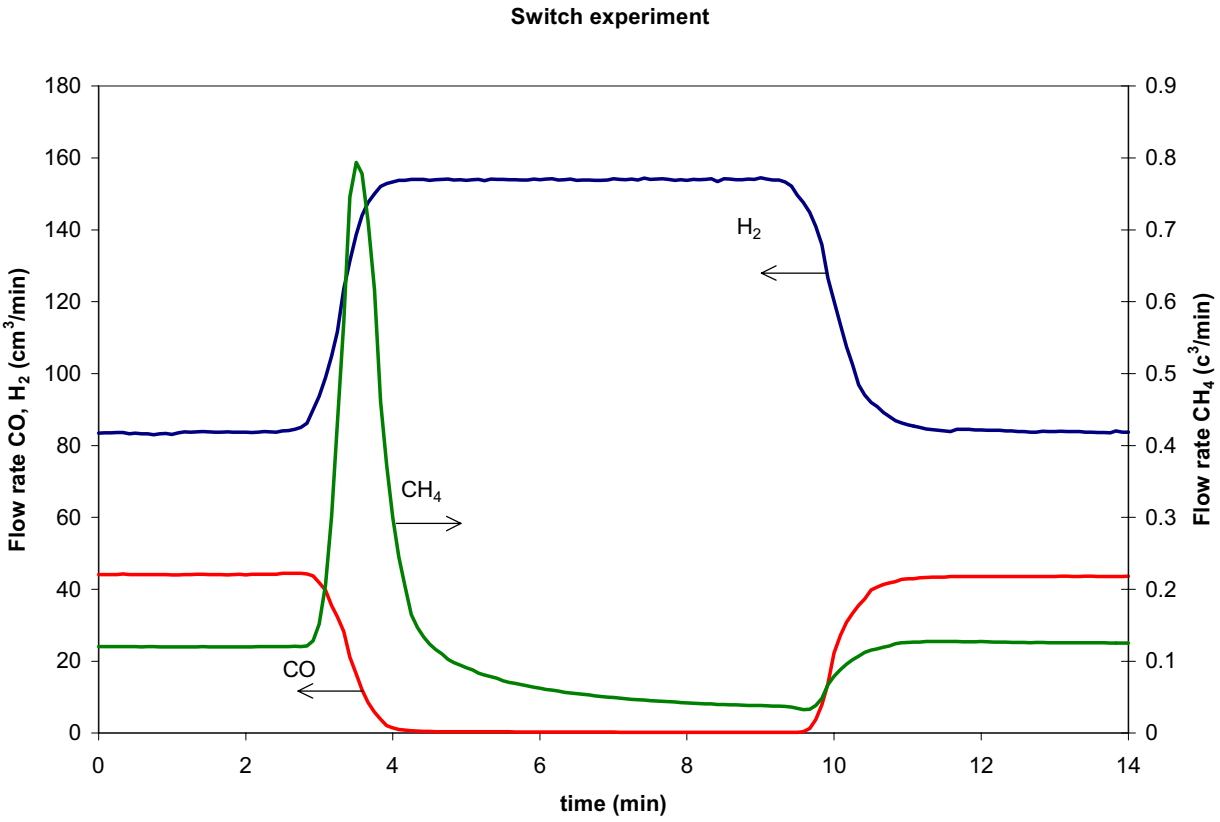

Figure II.3 - Switch from CO to H_2 (flow rate = 150 cm^3/min, T = 465 K, P = 580 kPa)

By assuming that all the methane detected after the switch to hydrogen was formed by hydrogenation of the carbon present on the catalyst surface, it was possible to estimate the percentage coverage of the catalyst by that carbon θ_C by integrating the CH_4 peak:

$$\theta_C = \frac{PM_{Co}}{W_{cat} \cdot P_{Co} \cdot D} \int \left[F_{CH_4}(t) - B(t) \right] dt \tag{II.3}$$

where PM_{Co} is the molecular weight of cobalt (g/mol), W_{cat} the loaded amount of catalyst (g), P_{Co} the weight percentage of Co on the catalyst, D the dispersion of the catalyst, $F_{CH4}(t)$ the actual flow rate of methane during the transient, $B(t)$ a baseline calculated by applying equation (II.1) to methane with the fluid dynamic time constant estimated from the dynamics of the internal standard (He).
The peak and the baseline are shown in more detail in Figure II.4.

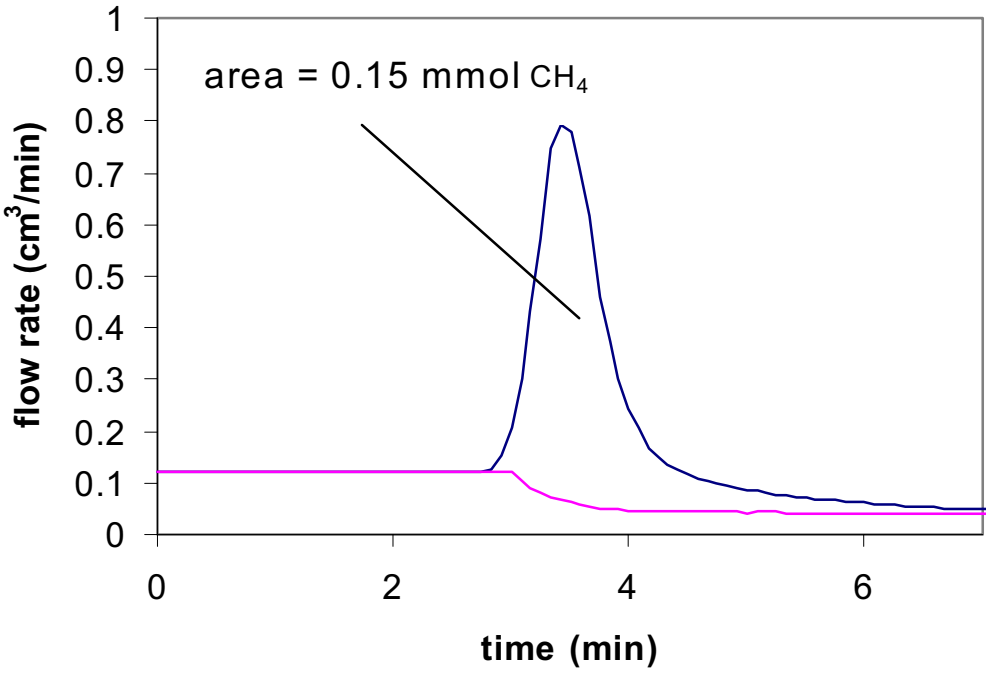

Figure II.4 - CH_4 peak after the switch (flow rate = 150 cm^3/min, T = 465 K, P = 580 kPa)

The time constant τ used to calculate the baseline was the one estimated from the transient of He after the switch (τ = 20 s). The carbon coverage θ_C estimated from equation (II.3) was 18.6%. The same experiment was repeated to verify the reproducibility of the data. From this second experiment, a θ_C of 18.4% was estimated, very similar to the previous one. The fluid dynamics of the descent of methane concentration after the maximum can be modeled using equation (II.1) by calculating a specific time constant τ_{CH4}. For this first test though, it seems that the curve presents two different time constants: a smaller one closer to the maximum (25 s) and a larger one for times greater than ~ 4.6 min (100 s). This suggests the presence of two different pools of adsorbed carbon, one of which is more reactive to hydrogen than the other.

Data at different operative conditions were then collected. Because of technical problems, it was not possible to make online GC analyses before these new experiments, and therefore it was not possible to obtain a direct estimate of the flow rate of methane going to the MS. Nevertheless, it is known that on increasing the bed residence time of synthesis gas, CO conversion increases and methane selectivity decreases: this is a reflection of the fact that the CO consumption rate is enhanced, whereas the CH_4 formation rate remains almost constant. For this reason, it is not

unreasonable to estimate the same flow rate of methane downstream the reactor even for different space velocity than the one just presented (syngas flow rate of 150 cm^3/min, corresponding to a space velocity of 150 cm^3/g/min and a bed residence time of 0.40 s).
With this assumption it was possible to estimate the carbon coverage at different residence time (i.e. different CO conversion and CH_4 selectivity).
The results of those new experiments are reported in Table II.1.

Table II.1 - Switch experiments at different space velocity

F (cm^3/min)	T (K)	P (kPa)	residence time (s)	ξ_{CO}	s_{CH4}	τ (s)	$\tau_{CH4,1}$ (s)	$\tau_{CH4,2}$ (s)	θ_C
150	465	580	0.40	5%	6%	0.35	25	100	18.6%
150	465	580	0.40	5%	6%	0.35	28	76	18.4%
100	465	650	0.60	-	-	0.35	32	95	33.3%
76	465	650	0.79	-	-	0.35	44	91	51.7%

In Table II.1 ξ_{CO} is the CO conversion, s_{CH4} is the selectivity to methane, τ is the time constant estimated from the fluid dynamic transient of the internal standard (He), whereas $\tau_{CH4,1}$ and $\tau_{CH4,2}$ are the two time constants estimated for the descent of methane after the maximum of the peak. While the fluid dynamics of the transient are not affected by the change of the bed residence time, the carbon coverage is quite different. The value of θ_C increases with increasing the bed residence time.
This trend can actually be affected by the assumption made that the methane flow rate to the MS is constant. Also, the values of θ_C can be overestimated, since part of the methane evolved can be formed not from hydrogenation of the carbon pool adsorbed on the catalyst surface, but from hydrogenation of gaseous CO not yet removed from the reactor gas phase after the switch. In fact before all the CO is removed from the reactor, the H_2/CO ratio in the reactor is high and can lead to significant methanation of the gas phase CO.

2. In situ FTIR Studies to Study the Water Effect

Experimental Approach

In situ FTIR spectroscopic measurements initiated during the previous quarter [26] were completed during the current reporting period. These experiments were performed using a RS-18000 Mattson Spectrometer. A stainless steel transmission infrared cell was used for all experiments. The sample was in the form of a thin wafer, placed in a specially designed holder at the middle of the cell, and the gas phase volume in the cell was minimized by the use of CaF_2 windows on either side of the pellet holder. The cell was heated to the required temperature using a heating coil wrapped around the cell. The two ends of the cell were cooled by circulating water flowing in a separate chamber at 353 K.

Co/SiO_2 (70 mg, 12.7 wt.%) diluted with Alon Al_2O_3 (30 mg) was pressed to a wafer 20 mm in diameter and approximately 1 mm thick. The sample was treated in a flow of O_2/He at 623 K for

30 min to remove any hydrocarbons. After briefly flushing with He to remove O_2 in the lines, the sample was reduced in H_2 at 623 K for 2 h. It was then cooled to 453 K before the FTS experiments. The ramping and cooling rate of the cell was maintained at 5 K/min a rate low enough to protect the CaF_2 windows from cracking. A background of the sample at 453 K in H_2 was collected prior to the experiments, which were performed at 453 K and 473 K, 500 kPa and H_2/CO=2 (CO=30 cc/min, H_2=60 cc/min). Addition of water was performed using an Isco 500 D series syringe pump. Transmission IR spectra were collected with a resolution of 2 cm^{-1}. All spectra collected thus were processed to be free of any interference from gas phase CO peaks by subtraction with a standard CO gas phase spectrum.

Results and Discussion

In situ FTIR spectra collected on the Co/SiO_2 sample at 473 K and 500 kPa (H_2/CO=2) at 1 min and 68 min (steady state) are shown in Figure II-5. The peak at 1590 cm^{-1} (symmetric –OCO- stretching vibrations) coupled with a doublet at 1390 (-CH deformation mode) and 1377 cm^{-1} (asymmetric –OCO- stretching vibrations), which are masked due to the strong intensity of hydroxyls on SiO_2, are attributed to surface formates. The peak at 2067 cm^{-1} is characteristic of linearly bonded –CO stretching vibrations on cobalt sites [27,28]. This peak moves and weakens to 2057 cm^{-1} with increasing time and reaches a constant intensity at steady state. In addition, the two intense bands observed at 2927 cm^{-1} and 2855 cm^{-1} have previously been assigned to symmetric and asymmetric C-H vibrations in methylene groups, while the weak shoulder at 2959 cm^{-1} can be assigned to C-H stretching vibrations in methyl groups [28-30]. As observed in Figure II-5, these bands increase in intensity as a function of time, indicating that these correspond to hydrocarbon chains formed during the reaction. As reported earlier, these bands are not reaction products adsorbed from the gas phase but adspecies formed during the reaction, based on previously studies with adsorption of molecules from gas phase [28]. In addition, there is also a weak band around 1900 cm^{-1}, which is characteristic of bridged –CO- stretching vibrations on Co sites.

The experiment was conducted as shown in Table II-2. The area under the CO adsorption peak is plotted as a function of cumulative time in contact with synthesis gas in Figure II-6. Spectra were collected at 453 K, 500 kPa without added water and continued to run until attainment of steady state. The temperature was then increased to 473 K. The area of the CO adsorption band reached a value of ~29.8 (b). Water at 50 kPa and 100 kPa were subsequently added to synthesis gas and spectra were collected until steady state was reached. The area under the band increased by 15% upon addition of 50 kPa water (c) and a further 5% upon increasing the water partial pressure to 100 kPa (d). The CO adsorption band shifted to lower wavenumbers (~2050 cm^{-1}) and an intense band appeared at 1628 cm^{-1}, which was assigned to adsorbed water (Figure II-7). This band at 1628 cm^{-1} was also present when the experiment was conducted on the pure SiO_2 support, with added water, indicating that this was characteristic of adsorbed water on the support. When water flow was stopped, the spectra did not revert back to the original conditions both in terms of CO adsorption peak area or wavenumber (e), with the exception of the gradual disappearance of the water adsorption peak.

The temperature was decreased back to 453 K (f) and water addition of 50 kPa and 100 kPa was performed the same way as before. The CO adsorption peak did not show a significant increase

(g), and in fact showed a decrease in peak area when 100 kPa water was added (h), indicating excessive adsorption of water covering some of the active sites available for CO adsorption. Hence water flow was instantly switched off to prevent catalyst deactivation. Immediately after the water flow was stopped the CO adsorption peak reverted back to the original condition (f), which indicated that the catalyst had changed from its initial condition (a). Finally the addition of 200 kPa or 300 kPa water leads to catalyst deactivation and the area of the CO adsorption peak decreased to zero indicating the complete oxidation of the catalyst and the disappearance of Co metal sites capable of binding CO.

Our results indicated that the significant promotion of the FT rate in the presence of water as observed during our reaction studies could not be explained as being just due to an increase in the total number of sites available for CO adsorption. This suggests that the autocatalytic effect of water may be due to the participation of water as a reactant in kinetically relevant steps in the FT reaction mechanism. Furthermore, the fact that the conditions (f) and (a) are so different from each other indicated an irreversible modification of the Co structure when water is introduced for the first time onto the catalyst surface.

Hence, these experiments will be conducted during the next reporting period, in the exact same manner in a plug-flow microreactor on this Co/SiO_2 catalyst, at identical conditions, *i.e.*, 473 K and 453 K, 500 kPa, in order to confirm whether the structure of CO is modified when water is present near the surface of the catalyst. These experiments coupled with the switching experiments both in the presence and absence of water (already in progress) will provide a clearer picture on the effect of water on the performance of Co-FTS catalysts.

Table II.2 – Conditions for in situ FTIR spectroscopic experiments

Condition	Description
(a)	453 K, no water, run to steady state
(b)	473 K, no water, run to steady state
(c)	473 K, 50 kPa water, run to steady state
(d)	473 K, 100 kPa water, run to steady state
(e)	473 K, water stopped, run to steady state
(f)	Temperature lowered to 453 K, steady state
(g)	453 K, 50 kPa water, run to steady state
(h)	453 K, 100 kPa, water
(i)	453 K, water stopped
(j)	453 K, 200-300 kPa water

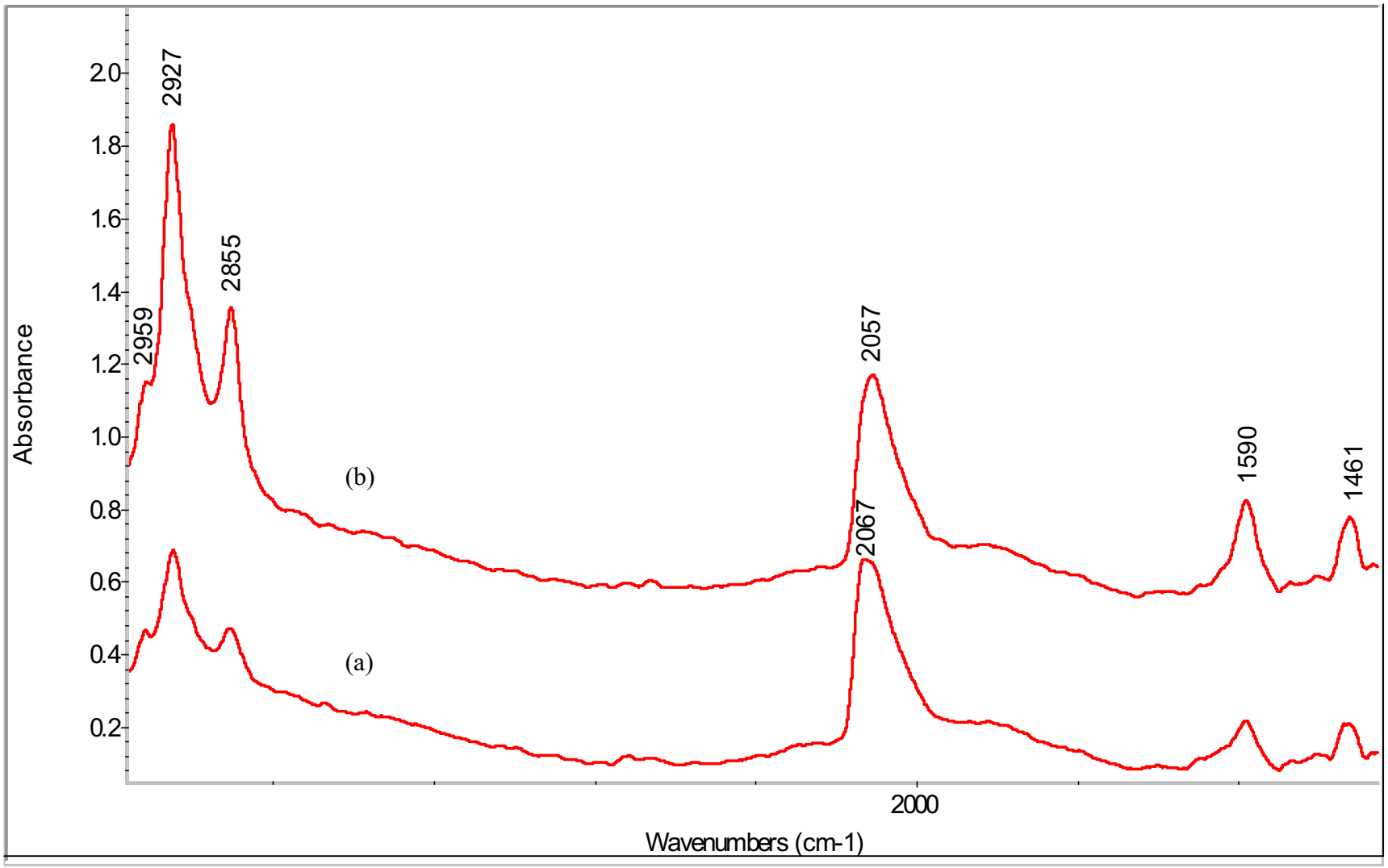

Figure II. 5. *In situ* FTIR spectra of a 12.7% Co/SiO_2 catalyst at 473 K, 500 kPa, a) 1 min, b) 68 min (steady state).

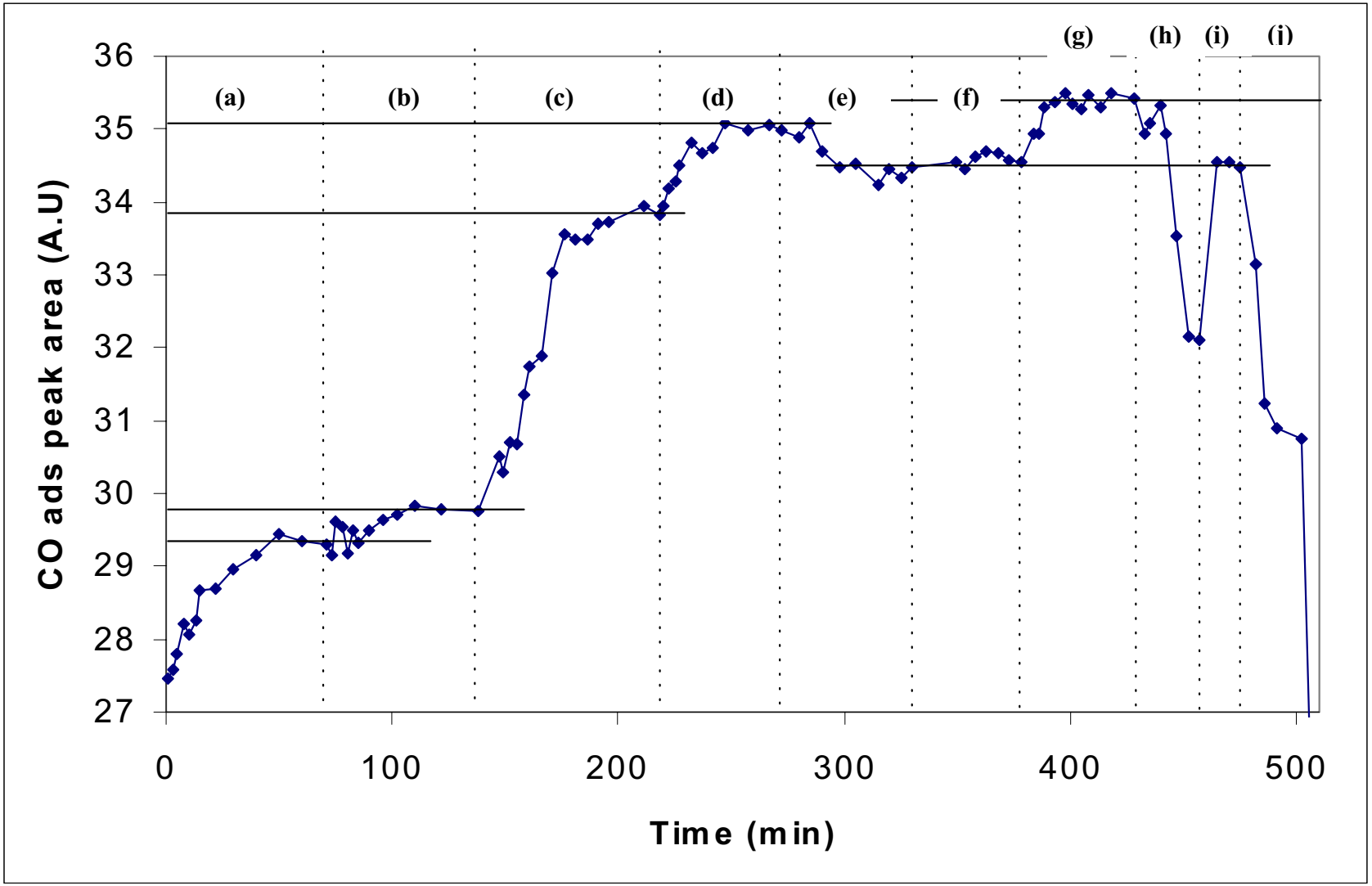

Figure II-7. Area of CO adsorption peak as a function of cumulative time. Conditions as in Table II-2.

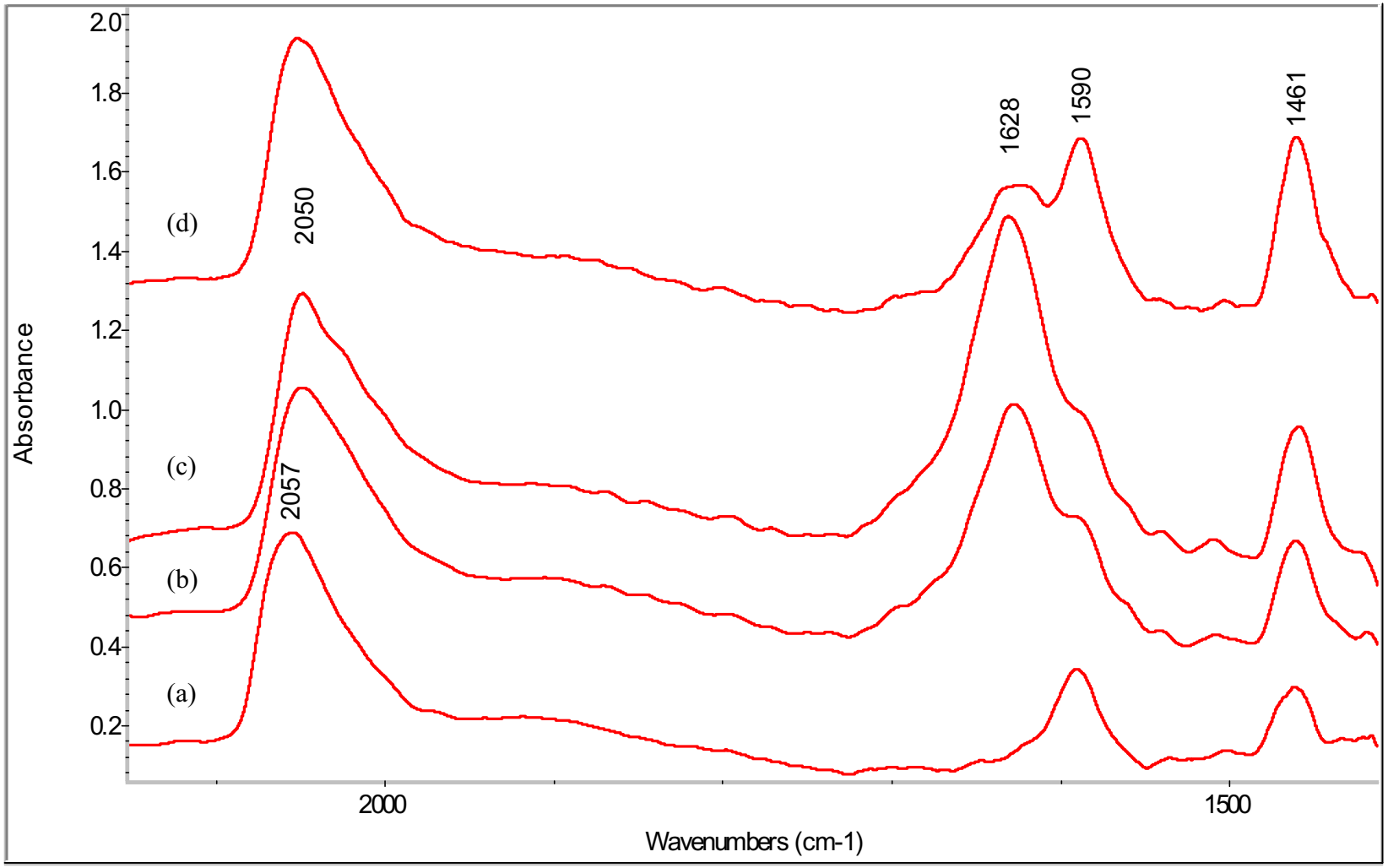

Figure II. 6. Steady state *in situ* FTIR spectra of a 12.7% Co/SiO_2 catalyst at a) 473 K, 500 kPa, b) 473 K, 50 kPa water, c) 100 kPa water and d) water stopped.

II. APPENDIX

1. References

1. M. E. Dry, The Fisher-Tropsch Synthesis, in *Catalysis-Science and Technology*, Vol. 1, p. 160, J. R. Anderson and M. Boudart eds., Springer Verlag, New York, 1981.
2. F. Fischer and H. Tropsch, *Brennstoff-Chem.* 7 (1926) 97.
3. R. B. Anderson, in *Catalysis* Vol. 4, p. 29, P. H. Emmett eds., Van Nostrand-Reinhold, New York, 1956.
4. H. H. Storch, N. Golumbic and R. B. Anderson, *The Fischer-Tropsch and Related Syntheses*, Wiley, New York, 1951; R. B. Anderson, *The Fischer-Tropsch Synthesis*, Wiley, New York, 1984.
5. H. Kolbel and M. Ralek, *Catal. Rev.-Sci. Eng.* 21 (1980) 225.
6. J. W. Niemantsverdriet and A. M. van der Kraan, *J. Catal.* 72 (1981) 385.
7. J. A. Amelse, J. B. Butt and L. J. Schwartz, *J. Phys. Chem.* 82 (1978) 558.
8. G. B. Raupp and W. N. Delgass, *J. Catal.* 58 (1979) 348.
9. R. Dictor and A. T. Bell, *J. Catal.* 97 (1986) 121.
10. J. P. Reymond, P. Meriaudeau and S. J. Teichner, *J. Catal.* 75 (1982) 39.
11. C. S. Kuivila, P. C. Stair and J. B. Butt, *J. Catal.* 118 (1989) 299.
12. C. S. Huang, L. Xu and B. H. Davis, *Fuel Sci. Tech. Int.* 11 (1993) 639.
13. S. Soled, E. Iglesia and R. A. Fiato, *Catal. Lett.* 7 (1990) 271.
14. S. Soled, E. Iglesia, S. Miseo, B. A. DeRites and R. A. Fiato, *Topics in Catal.* 2 (1995) 193.
15. E. Iglesia, A research proposal submitted to the Division of Fossil Energy.
16. R. J. O'Brien, L. Xu. R. L. Spicer and B. H. Davis, *Energy and Fuels*, 10 (1996) 921.
17. D. B. Bukur, D. Mukesh, and S. A. Patel, *Ind. Eng. Chem. Res*., 29, 194 (1990).
18. 1st Quarterly report, 1999. U.S. Department of Energy under contract # DE-FC26-98FT40308.
19. 2nd Quarterly report, 1999. U.S. Department of Energy under contract # DE-FC26-98FT40308.
20. 3rd Quarterly report, 1999. U.S. Department of Energy under contract # DE-FC26-98FT40308.
21. 4th Quarterly report, 1999. U.S. Department of Energy under contract # DE-FC26-98FT40308.
22. 1st Quarterly report, 2000. U.S. Department of Energy under contract # DE-FC26-98FT40308.
23. 2nd Quarterly report, 2000. U.S. Department of Energy under contract # DE-FC26-98FT40308.
24. 3rd Quarterly report, 2000. U.S. Department of Energy under contract # DE-FC26-98FT40308.
25. 4th Quarterly report, 2000. U.S. Department of Energy under contract # DE-FC26-98FT40308.
26. 1st Quarterly report, 2001. U.S. Department of Energy under contract # DE-FC26-98FT40308.
27. R. A. Dalla Betta, and M. Shelef, *J. Catal*., 48 (1977)111.
28. J. G. Ekerdt and A. T. Bell, *J. Catal*., 58 (1979) 170.
29. D. L. King, *J. Catal*., 61 (1980) 77.

30. L. J. Bellamy, “The Infrared Spectra of Complex Molecules”, 3rd Ed., Wiley, New York, 1975.

Task 12. Reporting/Project Management

Three monthly and one quarterly reports have been completed.